

**A Study of the Semileptonic Charm Decays  $D^0 \rightarrow \pi^- e^+ \nu_e$ ,  $D^+ \rightarrow \pi^0 e^+ \nu_e$ ,  $D^0 \rightarrow K^- e^+ \nu_e$ ,  
and  $D^+ \rightarrow \bar{K}^0 e^+ \nu_e$**

S. Dobbs, Z. Metreveli, K. K. Seth, and A. Tomaradze  
*Northwestern University, Evanston, Illinois 60208*

J. Ernst  
*State University of New York at Albany, Albany, New York 12222*

H. Severini  
*University of Oklahoma, Norman, Oklahoma 73019*

S. A. Dytman, W. Love, and V. Savinov  
*University of Pittsburgh, Pittsburgh, Pennsylvania 15260*

O. Aquines, Z. Li, A. Lopez, S. Mehrabyan, H. Mendez, and J. Ramirez  
*University of Puerto Rico, Mayaguez, Puerto Rico 00681*

G. S. Huang, D. H. Miller, V. Pavlunin, B. Sanghi, I. P. J. Shipsey, and B. Xin  
*Purdue University, West Lafayette, Indiana 47907*

G. S. Adams, M. Anderson, J. P. Cummings, I. Danko, and J. Napolitano  
*Rensselaer Polytechnic Institute, Troy, New York 12180*

Q. He, J. Insler, H. Muramatsu, C. S. Park, E. H. Thorndike, and F. Yang  
*University of Rochester, Rochester, New York 14627*

T. E. Coan, Y. S. Gao, and F. Liu  
*Southern Methodist University, Dallas, Texas 75275*

M. Artuso, S. Blusk, J. Butt, J. Li, N. Menea, R. Mountain, S. Nisar, K. Randrianarivony,  
R. Redjimi, R. Sia, T. Skwarnicki, S. Stone, J. C. Wang, and K. Zhang  
*Syracuse University, Syracuse, New York 13244*

S. E. Csorna  
*Vanderbilt University, Nashville, Tennessee 37235*

G. Bonvicini, D. Cinabro, M. Dubrovin, and A. Lincoln  
*Wayne State University, Detroit, Michigan 48202*

D. M. Asner and K. W. Edwards  
*Carleton University, Ottawa, Ontario, Canada K1S 5B6*

R. A. Briere, I. Brock, J. Chen, T. Ferguson, G. Tatishvili, H. Vogel, and M. E. Watkins  
*Carnegie Mellon University, Pittsburgh, Pennsylvania 15213*

J. L. Rosner  
*Enrico Fermi Institute, University of Chicago, Chicago, Illinois 60637*

N. E. Adam, J. P. Alexander, K. Berkelman, D. G. Cassel, J. E. Duboscq, K. M. Ecklund, R. Ehrlich, L. Fields,  
L. Gibbons, R. Gray, S. W. Gray, D. L. Hartill, B. K. Heltsley, D. Hertz, C. D. Jones, J. Kandaswamy,  
D. L. Kreinick, V. E. Kuznetsov, H. Mahlke-Krüger, P. U. E. Onyisi, J. R. Patterson, D. Peterson, J. Pivarski,  
D. Riley, A. Ryd, A. J. Sadoff, H. Schwarthoff, X. Shi, S. Stroiney, W. M. Sun, T. Wilksen, and M. Weinberger  
*Cornell University, Ithaca, New York 14853*

S. B. Athar, R. Patel, V. Potlia, and J. Yelton  
*University of Florida, Gainesville, Florida 32611*

P. Rubin

*George Mason University, Fairfax, Virginia 22030*

C. Cawlfeld, B. I. Eisenstein, I. Karliner, D. Kim, N. Lowrey, P. Naik, C. Sedlack, M. Selen, E. J. White, and J. Wiss  
*University of Illinois, Urbana-Champaign, Illinois 61801*

M. R. Shepherd

*Indiana University, Bloomington, Indiana 47405*

D. Besson

*University of Kansas, Lawrence, Kansas 66045*

T. K. Pedlar

*Luther College, Decorah, Iowa 52101*

D. Cronin-Hennessy, K. Y. Gao, D. T. Gong, J. Hietala, Y. Kubota,  
T. Klein, B. W. Lang, R. Poling, A. W. Scott, A. Smith, and P. Zweber  
*University of Minnesota, Minneapolis, Minnesota 55455*

(CLEO Collaboration)

(Dated: December 5, 2007)

Using a sample of 1.8 million  $D\bar{D}$  mesons collected at the  $\psi(3770)$  with the CLEO-c detector, we study the semileptonic decays  $D^0 \rightarrow \pi^- e^+ \nu_e$ ,  $D^+ \rightarrow \pi^0 e^+ \nu_e$ ,  $D^0 \rightarrow K^- e^+ \nu_e$ , and  $D^+ \rightarrow \bar{K}^0 e^+ \nu_e$ . For the total branching fractions we find  $\mathcal{B}(D^0 \rightarrow \pi^- e^+ \nu_e) = 0.299(11)(9)\%$ ,  $\mathcal{B}(D^+ \rightarrow \pi^0 e^+ \nu_e) = 0.373(22)(13)\%$ ,  $\mathcal{B}(D^0 \rightarrow K^- e^+ \nu_e) = 3.56(3)(9)\%$ , and  $\mathcal{B}(D^+ \rightarrow \bar{K}^0 e^+ \nu_e) = 8.53(13)(23)\%$ , where the first error is statistical and the second systematic. In addition, form factors are studied through fits to the partial branching fractions obtained in five  $q^2$  ranges. By combining our results with recent unquenched lattice calculations, we obtain  $|V_{cd}| = 0.217(9)(4)(23)$  and  $|V_{cs}| = 1.015(10)(11)(106)$ , where the final error is theoretical.

PACS numbers: 12.15.Hh, 13.20.Fc, 14.40.Lb

## I. INTRODUCTION

In the standard model of particle physics, mixing of the quark mass eigenstates in their charged current interactions is described by the Cabibbo Kobayashi Maskawa (CKM) matrix [1]. This  $3 \times 3$  quark mixing matrix must be unitary and can be described by four independent parameters. If the standard model is complete, experimental determination of the CKM matrix elements should verify its unitarity. Deviations from unitarity would indicate the presence of physics beyond the standard model. A variety of  $CP$ -conserving and  $CP$ -violating observables probe the elements of the CKM matrix and allow us to over-constrain it. Many of the key observables require great precision or great sensitivity to provide the constraints at the level needed to test the validity of the standard model description. It thus remains a continuing experimental challenge to test the unitarity of the CKM matrix fully.

Study of the semileptonic decay of  $D$  mesons plays a primary role in our understanding of the CKM matrix. These decays allow robust determination of the CKM matrix elements  $|V_{cs}|$  and  $|V_{cd}|$  by combining measured branching fractions with form factor calculations, such as those based on unquenched lattice QCD (LQCD) [2]. In addition, these measurements will provide preci-

sion tests of LQCD itself [3]. One approach to tests of LQCD assumes unitarity of the CKM matrix and compares the constrained matrix elements [4] to elements obtained with a combination of CLEO-c measurements and lattice form factors. A second approach, which is independent of CKM elements and thus free from the unitarity assumption, compares the measured and calculated ratios of semileptonic and purely leptonic branching fractions. Verification of lattice calculations at the few percent level will provide validation for use of the lattice in the  $B$  system, where they are relied upon for several crucial theoretical quantities.

This article presents a study of the  $D^0 \rightarrow \pi^- e^+ \nu_e$ ,  $D^+ \rightarrow \pi^0 e^+ \nu_e$ ,  $D^0 \rightarrow K^- e^+ \nu_e$  and  $D^+ \rightarrow \bar{K}^0 e^+ \nu_e$  decay modes (charge conjugate modes implied). A summary of the analysis is also provided in a shorter companion article [5]. The results are based on a sample of 1.8 million  $DD$  pairs collected with the CLEO-c detector at the Cornell Electron Storage Ring (CESR) from  $281 \text{ pb}^{-1}$  of  $e^+e^-$  data at the  $\psi(3770)$  resonance. The sample is a superset of, and approximately five times larger than, the data used to obtain the first CLEO-c semileptonic branching fraction measurements [6]. For each mode we determine the partial branching fractions in five  $q^2$  ranges, with the sum of the five rates determining the total branching fraction. Fits to the rates de-

termine the form factor shapes. By incorporating LQCD calculations into the form factor fits, we extract values for the CKM elements  $|V_{cd}|$  and  $|V_{cs}|$ . Previous quenched lattice predictions carried errors of about 20%. Current unquenched LQCD calculations allow theoretical evaluation of the form factors at the 10% [2] level, with future improvement to the few percent level expected.

Within this article, Section II provides an overview of the formalism for exclusive semileptonic decays of charm mesons and their associated form factors. Sections III through VI cover the experimental procedures for event reconstruction and extraction of the branching fractions, the systematic uncertainty evaluation, and the branching fraction results. Sections VII and VIII explore the form factor shape constraints from our data and the extraction of  $|V_{cs}|$  and  $|V_{cd}|$ . Section IX presents our conclusions and comparisons with previous measurements.

## II. EXCLUSIVE CHARMED SEMILEPTONIC DECAYS

The matrix element describing the semileptonic decay of a  $D$  meson to a pseudoscalar meson  $P$  is of the form

$$\mathcal{M}(D \rightarrow Pe^+\nu_e) = -i\frac{G_F}{\sqrt{2}}V_{cq}^*L^\mu H_\mu, \quad (1)$$

where  $G_F$  is the Fermi constant,  $V_{cq}$  is the appropriate CKM matrix element and  $L^\mu$  and  $H_\mu$  are the leptonic and hadronic currents. The leptonic current can be written in terms of the electron and neutrino Dirac spinors,  $u_e$  and  $v_\nu$ ,

$$L^\mu = \bar{u}_e\gamma^\mu(1 - \gamma_5)v_\nu. \quad (2)$$

In the case of pseudoscalar decays, where there is no axial-vector contribution, the hadronic current is given by

$$H_\mu = \langle P(p)|\bar{q}\gamma_\mu c|D(p')\rangle, \quad (3)$$

where  $p'$  and  $p$  are the four-momenta of the parent  $D$  meson and the daughter  $P$  meson, respectively. The hadronic current is fundamentally a non-perturbative quantity that is difficult to evaluate. We can, however, re-parameterize the current by expressing it in terms of the independent four-momenta in the process, which for a pseudoscalar-to-pseudoscalar decay are the two four-momenta  $p' + p$  and  $q = p' - p$ . We can identify  $q$  as the four-momentum of the virtual  $W$  boson. A typical formulation of the hadronic current in terms of these four-momenta is given by

$$\begin{aligned} \langle P(p)|\bar{q}\gamma^\mu c|D(p')\rangle = & \quad (4) \\ f_+(q^2) \left[ (p' + p)^\mu - \frac{M_D^2 - m_P^2}{q^2} q^\mu \right] + & \\ f_0(q^2) \frac{M_D^2 - m_P^2}{q^2} q^\mu, & \end{aligned}$$

where  $M_D$  is the mass of the  $D$  meson and  $m_P$  is the mass of the final state pseudoscalar meson. The non-perturbative contributions are incorporated in the scalar functions  $f_+(q^2)$  and  $f_0(q^2)$ , the form factors of the decay. Kinematic constraints require  $f_+(0) = f_0(0)$ . A further simplification arises due to the small mass of the electron because  $q^\mu L_\mu \rightarrow 0$  in the limit  $m_e \rightarrow 0$ . Thus including only the  $f_+$  form factor in the hadronic current,

$$\langle P(p)|\bar{q}\gamma^\mu c|D(p')\rangle = f_+(q^2)(p' + p)^\mu, \quad (5)$$

is a very good approximation. With this form for the hadronic current the partial decay width becomes

$$\frac{d\Gamma(D \rightarrow Pe\nu_e)}{dq^2} = \frac{G_F^2|V_{cq}|^2}{24\pi^3} p^3 |f_+(q^2)|^2. \quad (6)$$

The partial decay width (Eq. 6) clearly reveals that extraction of the CKM matrix elements from measured rates requires prediction of the semileptonic form factors. Theoretical calculation of the form factors therefore has become a considerable industry. We focus here on parameterizations of the form factors that we employ in our form factor studies and in extraction of  $|V_{cd}|$  and  $|V_{cs}|$ .

The goal of any particular parameterization of the semileptonic form factors is to provide an accurate, and physically meaningful, expression of the strong dynamics in the decays. To that end, one may express the form factors in terms of a dispersion relation, an approach that has been well established in the literature (see for example Ref. [9] and references therein). It is common to write the dispersive representation in terms of an explicit pole and a sum of effective poles:

$$f_+(q^2) = \frac{f_+(0)}{1 - \alpha} \frac{1}{1 - \frac{q^2}{m_{\text{pole}}^2}} + \sum_{k=1}^N \frac{\rho_k}{1 - \frac{1}{\gamma_k} \frac{q^2}{m_{\text{pole}}^2}}, \quad (7)$$

where  $\rho_k$  and  $\gamma_k$  are expansion parameters. Given the underlying  $c \rightarrow q$  quark transition of the semileptonic decay, the mass  $m_{\text{pole}}$  is the mass of the lowest-lying  $c\bar{q}$  vector meson. The parameter  $\alpha$  gives the contribution from the vector meson pole at  $q^2 = 0$ . Using this dispersion relation the true form factor can be approximated to any desired degree of accuracy by keeping sufficient terms in the expansion. This approach has the drawback that the decay dynamics are not explicitly predicted. Additionally, experimental data have suggested the need for only a few parameters in the description of the form factor shape. It is therefore natural to seek simplifications of this parameterization that can still capture the correct dynamics.

Removing the sum over effective poles entirely, leaving only the explicit vector meson pole, provides one simplification route that is typically referred to as ‘‘nearest pole dominance’’ or ‘‘vector-meson dominance’’. The resulting ‘‘simple pole’’ parameterization of the form factor is given by

$$f_+(q^2) = \frac{f_+(0)}{\left(1 - \frac{q^2}{m_{\text{pole}}^2}\right)}. \quad (8)$$

Experimental data disagree with the physical basis for this approximation, since measurements of the parameter  $m_{\text{pole}}$  that fit the data do not agree with the expected vector meson masses [14]. Effectively, at low or medium values of  $q^2$  the spectrum is distorted compared to the simple pole model, receiving contributions from the continuum of effective poles above the lowest lying pole mass.

The modified pole, or Becirevic-Kaidalov (BK) parameterization [8], was proposed to address this problem. The parameterization keeps the first term from the effective pole expansion, while making simplifications such that the form factor can be expressed using only two parameters: the intercept  $f_+(0)$  and an additional shape parameter.<sup>1</sup> The parameterization is typically expressed in the form

$$f_+(q^2) = \frac{f_+(0)}{\left(1 - \frac{q^2}{m_{\text{pole}}^2}\right)\left(1 - \alpha \frac{q^2}{m_{\text{pole}}^2}\right)}. \quad (9)$$

This parameterization has recently been widely used in the extraction of semileptonic form factors from experimental measurements [16, 17, 18, 19]. In addition, some recent LQCD calculations of the form factor have relied on this parameterization for extrapolation and interpolation purposes [2, 13]. This scheme requires several assumptions to reduce the multiple parameters initially present (Eq. 7) to one. The BK ansatz assumes that the gluon hard-scattering contributions ( $\delta$ ) are close to zero and that scaling violations ( $\beta$ ) are close to unity, which may be succinctly expressed as

$$1 + 1/\beta - \delta \equiv \frac{(M_D^2 - m_P^2)}{f_+(0)} \left. \frac{df_+}{dq^2} \right|_{q^2=0} \sim 2. \quad (10)$$

Once again, however, the experimental data do not bear out these assumptions [14]. We should observe  $\alpha \sim 1.75$  in order to obtain  $1 + 1/\beta - \delta = 2$ , whereas the observed data are removed from such values by many standard deviations.

We note that both functional forms can provide adequate parameterizations of the data if their parameters are allowed to be non-physical. Without a physical underpinning for the parameterization, however, parameters obtained from theory and/or from different experiments may not agree if their form factor sensitivities differ as a function of  $q^2$ .

Our primary form factor shape analysis therefore utilizes a series expansion around  $q^2 = t_0$  that has been advocated by several groups for a physical description of heavy meson form factors [9, 10, 11, 12]. The series expansion is congruous with the dispersion relations, and is guaranteed to contain the true form factor, yet is still rich

enough to describe all variations that affect the physical observables.

To achieve a convergent series, the expansion is formulated as an analytic continuation of the form factor into the complex  $t = q^2$  plane. There is a branch cut on the real axis for  $t > (M_D + M_{K,\pi})^2$  that is mapped onto the unit circle by the variable  $z$ , defined as

$$z(q^2, t_0) = \frac{\sqrt{t_+ - q^2} - \sqrt{t_+ - t_0}}{\sqrt{t_+ - q^2} + \sqrt{t_+ - t_0}}, \quad (11)$$

where  $t_{\pm} \equiv (M_D \pm m_{K,\pi})^2$  and  $t_0$  is the (arbitrary)  $q^2$  value that maps to  $z = 0$ . The expression for the form factor becomes

$$f_+(q^2) = \frac{1}{P(q^2)\phi(q^2, t_0)} \sum_{k=0}^{\infty} a_k(t_0) [z(q^2, t_0)]^k, \quad (12)$$

with

$$P(q^2) \equiv \begin{cases} 1, & D \rightarrow \pi \\ z(q^2, M_{D_s}^2), & D \rightarrow K \end{cases}. \quad (13)$$

The  $P(q^2)$  factor accommodates sub-threshold resonances, which overcomes the convergence issues that a naive expansion would face with a nearby pole. Good convergence properties are expected since the physical region is restricted to  $|z| < 1$ . The physical observables do not depend on the choice of  $\phi(q^2, t_0)$ , which can be any analytic function, or on the value of  $t_0$ . We report  $a_k$  parameters that correspond to  $t_0 = 0$  and the “standard” choice for  $\phi$  (see, *e.g.* Ref. [12] and Appendix A), which results from bounding  $\sum a_k^2$  from unitarity considerations. Appendix A presents results for an alternate choice of  $t_0$  that minimizes the maximum value of  $|z|$  over the physical range. If the series converges quickly, as expected, it is likely that only the first two or three terms will be able to be seen in the data. We will explore the number of terms needed to adequately describe our data.

While our primary form factor and CKM results will be based on the series expansion, we will also provide results based on the two pole parameterizations for comparative purposes.

### III. EVENT RECONSTRUCTION AND SELECTION

The analysis technique rests upon association of the missing energy and momentum in an event with the neutrino four-momentum [20], an approach enabled by the excellent hermeticity and resolution of the CLEO-c detector [3, 21]. Charged particles are detected over 93% of the solid angle by two wire tracking chambers within a 1.0 T solenoid magnet. The momentum resolution is 0.6% at 800 MeV/c. Specific ionization measurements from the tracking system in combination with a ring imaging Čerenkov detector (RICH) [22] provide particle identification. A CsI(Tl) crystal electromagnetic

<sup>1</sup> There will be three parameters if the  $f_0(q^2)$  form factor, which we are neglecting due to the small electron mass, is also taken into account.

calorimeter provides coverage over about 93% of  $4\pi$ , and achieves a typical  $\pi^0$  mass resolution of  $6 \text{ MeV}/c^2$ .

Electron candidates are identified above  $200 \text{ MeV}/c$  over 90% of the solid angle by combining information from specific ionization with calorimetric, RICH and tracking measurements. The identification efficiency, which has been determined from data, is greater than 96% above  $500 \text{ MeV}/c$  and greater than 90% above  $300 \text{ MeV}/c$ . The average probability that a hadron is misidentified as an electron is less than 0.8%. Below  $300 \text{ MeV}/c$  the efficiency falls rapidly, reaching 60% in the  $200 - 250 \text{ MeV}/c$  region. To reduce our sensitivity to final state radiation (FSR), we add photons within  $3.5^\circ$  of the initial electron momentum back into the tracking-based four-momentum.

Charged pions and kaons from the signal decay are identified using specific ionization and RICH measurements. Pion candidates below  $750 \text{ MeV}/c$  and kaon candidates below  $500 \text{ MeV}/c$  are identified using only specific ionization information, which is required to be within three standard deviations ( $\sigma$ ) of that expected for the assigned particle type. For pion candidates above  $650 \text{ MeV}/c$ , we also require the pion mass hypothesis be more likely than the kaon mass hypothesis. Above these momenta, candidate tracks must also pass RICH identification criteria. Specifically, we require that pion (kaon) candidates are more than  $3\sigma$  closer to a pion (kaon) hypothesis than a kaon (pion) hypothesis.

A  $\pi^0$  candidate must have a  $\gamma\gamma$  mass within  $2.5\sigma$  of the  $\pi^0$  mass.  $K_S^0$  candidates are reconstructed using a constrained vertex fit to candidate  $\pi^+\pi^-$  daughter tracks. The  $\pi^+\pi^-$  mass must be within  $4.5\sigma$  of the  $K_S^0$  mass.

To reconstruct the undetected neutrino we utilize the hermeticity of the CLEO-c detector to find the missing energy and momentum. In the process  $e^+e^- \rightarrow \psi(3770) \rightarrow D\bar{D}$ , the total energy of the beams is imparted to the  $D\bar{D}$  system. Because the beam energies are symmetric and the beam crossing angle is small at CESR, each produced  $D$  has an energy of the beam energy to within a small correction. The missing four-momentum in an event is given by  $p_{\text{miss}} = (E_{\text{miss}}, \vec{p}_{\text{miss}}) = p_{\text{total}} - \sum p_{\text{charged}} - \sum p_{\text{neutral}}$ , where the event four-momentum  $p_{\text{total}}$  is known from the energy and crossing angle of the CESR beams. Charged and neutral particles for the sums must pass selection criteria designed to achieve the best possible  $|\vec{p}_{\text{miss}}|$  resolution by balancing the efficiency for detecting true particles against the rejection of false ones.

For the charged four-momentum sum,  $\sum p_{\text{charged}}$ , optimal selection is achieved with topological criteria. These criteria minimize multiple-counting that can result from low-momentum tracks that curl in the magnetic field, charged particles that decay in flight or interact within the detector, and spurious tracks. Tracks that are actually segments of a single low transverse momentum ‘‘curling’’ particle are identified by selecting reconstructed track pairs with opposite curvature whose innermost and outermost diametric radii each match within 14 cm and whose separation in  $\phi$  is within  $180^\circ \pm 20^\circ$ . For physics

use we select the track segment that will best represent the original charged particle based on track quality and distance-of-closest-approach to the beam spot. We employ similar algorithms to identify particles that curl more than once, creating three or more track segments. We also identify tracks that have scattered or decayed in the drift chamber, causing the original track to end and one or more tracks to begin in a new direction. We keep only the track segment with the majority of its hits before the interaction point. Spurious tracks are identified by their low hit density and/or low number of overall hits and rejected.

Each hadronic track must be assigned a mass hypothesis to calculate its contribution to the total energy sum. We assign a most probable mass hypothesis by combining detector measurement with particle production information. The production information is introduced because it is only statistically advantageous to identify a track as a kaon at a momentum where many more pions than kaons are produced when the detector’s particle ID information strongly favors a kaon. For each track, we first calculate a likelihood for the kaon and pion hypothesis based on specific ionization and RICH measurements. Those likelihoods are then weighted by the Monte Carlo (MC) prediction for the relative  $K^-$  and  $\pi^-$  abundances in  $D$  decays at that track’s momentum, which then gives us the true probability for each mass hypothesis.

For the neutral four-momentum sum,  $\sum p_{\text{neutral}}$ , clusters resulting from the interactions of charged hadrons must be avoided. As a first step, calorimeter showers passing the standard CLEO proximity-matching (within 15 cm of a charged track) are eliminated. Optimizations also revealed that all showers under 50 MeV should be eliminated. The processes that result in reconstructed showers (‘‘splitoffs’’) separate from but within about  $25^\circ$  of a proximity-matched shower tend to result in an energy distribution over the  $3 \times 3$  central array of the splitoff shower that ‘‘points back’’ to the core hadronic shower. We combine this information with the ratio of energies in the  $3 \times 3$  to  $5 \times 5$  arrays of crystals, whether the shower forms a good  $\pi^0$ , and the MC predictions for relative spectra for true photons versus splitoff showers to provide an optimal suppression of the contribution.

Association of the missing four-momentum with the neutrino four-momentum is only accurate if the event contains no more than one neutrino and if all true particles are detected. For events with additional missing particles or doubly-counted particles, the signal modes tend not to reconstruct properly while background processes tend to smear into our sensitive regions. Hence, it is worthwhile to reject events for which independent measures indicate these problems. We therefore exclude events that have either more than one electron or non-zero net charge. Multiple electrons indicate an increased likelihood for multiple neutrinos, while non-zero net charge indicates at least one missed or doubly-counted charged particle.

After application of the above criteria approximately

90% of the signal MC  $|\vec{p}_{\text{miss}}|$  distribution is contained in a central core with  $\sigma \sim 15$  MeV/ $c$ .

To further enhance the association of the missing momentum with an undetected neutrino in our final event sample, we require that the  $M_{\text{miss}}^2 \equiv E_{\text{miss}}^2 - |\vec{p}_{\text{miss}}|^2$  be consistent with a massless neutrino. The  $M_{\text{miss}}^2$  resolution,

$$\sigma(M_{\text{miss}}^2) = 2E_{\text{miss}}\sigma(E_{\text{miss}}) \oplus 2|\vec{p}_{\text{miss}}|\sigma(|\vec{p}_{\text{miss}}|),$$

is dominated by the  $E_{\text{miss}}$  term since the resolution of  $|\vec{p}_{\text{miss}}|$  is roughly half that of  $E_{\text{miss}}$ . MC simulation indicated an optimal requirement of  $|M_{\text{miss}}^2/2|\vec{p}_{\text{miss}}|| < 0.2$  GeV/ $c^3$ , which (noting  $E_{\text{miss}} \approx |\vec{p}_{\text{miss}}|$  for signal) provides selection at approximately constant  $E_{\text{miss}}$  resolution. Additionally, because of the superior  $|\vec{p}_{\text{miss}}|$  resolution, in subsequent calculations we take  $p_\nu \equiv (|\vec{p}_{\text{miss}}|, \vec{p}_{\text{miss}})$ .

Semileptonic decays  $D \rightarrow Pe\nu$ , where  $P$  is a pion or kaon, are identified by their consistency with the expected  $D$  energy and momentum. Candidates are selected based on  $\Delta E \equiv (E_P + E_e + E_\nu) - E_{\text{beam}}$  (expected to be zero within our resolution of about 20 MeV) and yields are extracted from the resulting distributions in beam-constrained mass  $M_{\text{bc}}$  (equivalent to  $D$  momentum and expected to be close to the known  $D$  mass). These quantities are corrected for the small boost resulting from the 3 mrad beam crossing angle. Because the  $|\vec{p}_\nu|$  resolution dominates the  $\Delta E$  resolution, we can improve our  $p_\nu$  measurement by scaling it by the factor  $\zeta$  satisfying  $(E_P + E_e + \zeta E_\nu) - E_{\text{beam}} = 0$ . We use  $\zeta \vec{p}_\nu$  for the neutrino momentum in computation of  $M_{\text{bc}} \equiv \sqrt{E_{\text{beam}}^2 - |\vec{p}_P + \vec{p}_e + \zeta \vec{p}_\nu|^2}$ . The resulting resolution for  $M_{\text{bc}}$  is 4 MeV/ $c^2$ .

Selection criteria were optimized by studying MC samples independent of those used elsewhere in the analysis. Sources of backgrounds include events with fake electrons, non-charm continuum production ( $e^+e^- \rightarrow q\bar{q}$ ,  $e^+e^- \rightarrow \tau^+\tau^-$  and  $e^+e^- \rightarrow \gamma\psi(2S)$ ), and  $D\bar{D}$  processes other than signal.

The optimal  $\Delta E$  requirement was determined to be  $-0.06 < \Delta E < 0.10$  GeV. For the Cabibbo-favored modes, the background level remaining after this selection is only a few percent of the signal level. For the Cabibbo-suppressed modes, there remains significant background from cross-feed among the signal modes, particularly from the kaon modes, as well as from the related modes  $D^+ \rightarrow K_L^0 e^+ \nu_e$  and  $D^+ \rightarrow K_S^0 e^+ \nu_e$  where  $K_S^0 \not\rightarrow \pi^+ \pi^-$ . Since the cross-feed typically involves particles from the ‘‘other  $D$ ’’ decay, we obtain some suppression of this background with a  $q^2$ -dependent requirement on  $\Delta E_{\text{n.s.}}$  for the non-signal particles in the event. We obtain  $\Delta E_{\text{n.s.}}$  by summing the energy of all non-signal particles in an event, even though we do not specifically reconstruct the non-signal  $D$  decay. This criterion effectively imposes an additional constraint on the quality of the reconstructed neutrino. We also require  $D^+ \rightarrow \pi^0 e^+ \nu_e$  candidates to have the smallest  $|\Delta E|$  compared to any other final state candidates in the event, and that these

events contain no reconstructed  $D^0 \rightarrow K^- e^+ \nu_e$  candidate. These criteria suppress cross-feed from the charged pion and kaon modes with almost no loss of true  $\pi^0 e^+ \nu_e$  decays. The average background level ( $q^2$ -dependent) in the pion modes is about 20% of the signal level.

To simplify the statistical interpretation of our results, as well as to suppress cross-feed from the Cabibbo-favored into the Cabibbo-suppressed modes, we limit the number of multiple entries per event such that a given event can contribute to at most one  $D^0$  or one  $D^+$  final state. For events with multiple  $D^+$  candidates or multiple  $D^0$  candidates satisfying  $M_{\text{bc}} > 1.794$  GeV/ $c^2$ , we choose the candidate with the smallest  $|\Delta E|$ , independent of  $q^2$ .

From the measured electron and the re-scaled neutrino four-momenta we calculate  $q^2 \equiv M_{W^*}^2$  from  $q^2 = (p_\nu + p_e)^2$ . The resulting resolution is 0.01 GeV $^2/c^4$ , independent of  $q^2$ .

## IV. EXTRACTION OF BRANCHING FRACTIONS

### A. Method and Binning

For each of the four signal modes we construct the  $M_{\text{bc}}$  distributions in five  $q^2$  ranges:  $q^2 < 0.4$  GeV $^2/c^4$ ,  $0.4 \leq q^2 < 0.8$  GeV $^2/c^4$ ,  $0.8 \leq q^2 < 1.2$  GeV $^2/c^4$ ,  $1.2 \leq q^2 < 1.6$  GeV $^2/c^4$  and  $q^2 \geq 1.6$  GeV $^2/c^4$ . These 20 distributions are fit simultaneously to extract the partial branching fraction for each interval. The total branching fraction is then obtained in each mode by summing its five partial branching fractions. Fitting in five  $q^2$  ranges minimizes the experimental sensitivity of the total branching fractions to form factor shape uncertainties, while simultaneous fitting of all four modes ensures self-consistent handling of the cross-feed backgrounds among the modes.

The fit utilizes a binned maximum likelihood approach extended to include the finite statistics of the MC samples following the method of Barlow and Beeston [26]. The  $M_{\text{bc}}$  distribution is divided into fourteen uniform bins over the range  $1.794 < M_{\text{bc}} < 1.878$  GeV/ $c^2$ .

### B. Fit Components and Parameters

We fit the data to the signal components and five background components. The signal mode components are obtained from MC generated using EvtGen [24] and modified pole-model form factors [8] with parameters from the most recent LQCD results [2]. We apply several corrections to our GEANT-based [23] MC samples to improve simulation of the neutrino reconstruction procedure.

From independent studies, mostly based on CLEO-c samples with one fully reconstructed hadronic  $D$  decay, we evaluate corrections and associated systematic

uncertainties for simulation of hadronic showers, false charged particles and charged-particle identification. We find that the simulations of charged particles, charged-particle momentum resolution and photon-energy resolution need no correction, though we include the uncertainties in the systematic uncertainty evaluation. We reweight the MC samples to correct the rate and spectrum for  $K_L^0$  production (which affects the neutrino-reconstruction efficiency), for  $\pi^0$  and  $\pi^-$  production in our full  $D$  decay model, and for the momentum-dependent rate at which a  $K^-$  fakes a  $\pi^-$ . All of these corrections affect the cross-feed background rates into and between the Cabibbo-suppressed modes. They lead to few percent (or less) changes in the measured yields, but are determined to better than 10% of themselves.

In the MC samples we select only true electrons (reconstructed tracks that have been matched to a generator-level electron) with a probability for acceptance given by data-measured efficiencies described earlier. We thereby exclude from the MC any events caused by identification of a fake electron and instead estimate this background using data, as we describe in detail below. This procedure eliminates any reliance on MC predictions for either electron efficiency or the rate at which hadrons fake electrons.

We are sensitive to the distortion of efficiency and kinematics in our signal modes due to FSR. Based on the angular and energy distributions for FSR photons, we correct our signal MC, generated with the PHOTOS [27] package without interference effects included, to the Kaon Leading-Order Radiation (KLOR) [28] calculations modified for charm decay.

For each reconstructed  $q^2$  interval in a given mode, we generate a MC sample in the same (generator level)  $q^2$  interval, to which the full analysis is applied. That is, we obtain the full set of 20 reconstructed  $M_{bc}$  distributions from each of these 20 independent samples. For each of the generated  $q^2$  intervals, a single floating parameter, which corresponds to the efficiency-corrected data yield in that interval, controls the normalization of all its 20 reconstructed distributions. The relative normalizations among those reconstructed distributions remains fixed at the level predicted by our corrected MC. Because the signal rate in each reconstructed range drives the normalization for the corresponding generated  $q^2$  interval, the data in effect fixes the cross-feed rates into the other 19 reconstructed distributions.

We also use MC samples to describe the  $D\bar{D}$  background and the three continuum contributions. We absolutely scale the continuum components according to their cross sections at the  $\psi(3770)$  and the measured data luminosity. The non-signal  $D\bar{D}$  sample was generated using EvtGen, with decay parameters updated to reflect our best knowledge of  $D$  meson decays. This component floats separately for each reconstructed final state, but the relative rates over the five  $q^2$  regions within that state are fixed. This approach helps to reduce our sensitivity to inaccuracies in the  $D$  decay model. Fi-

nally, we input MC components for  $D^+ \rightarrow K_L^0 e^+ \nu_e$  and  $D^+ \rightarrow K_S^0(\pi^0 \pi^0) e^+ \nu_e$ , whose rates in each  $q^2$  region are tied to those for the signal  $D^+ \rightarrow K_S^0(\pi^+ \pi^-) e^+ \nu_e$  mode.

The contributions from events in which hadrons have faked the signal electron are evaluated using data. The momentum-dependent electron identification fake rates from pions and kaons are measured using a variety of data samples. We obtain our background estimates by analyzing a data sample with no identified electrons. Each track in each event in this sample is treated in turn as the signal electron. The contribution in each mode is then weighted according to the fake rate. The fake electron component is then added to the fit with a fixed, absolute, normalization.

Finally, we allow the fit to adjust the  $M_{bc}$  resolution in the  $D^0 \rightarrow \pi^- e^+ \nu_e$ ,  $D^+ \rightarrow \pi^0 e^+ \nu_e$ , and  $D^0 \rightarrow K^- e^+ \nu_e$  modes by applying a Gaussian smear to these distributions. As a result the signal MC  $M_{bc}$  resolution in these modes is increased from  $\sim 3.5$  MeV/ $c^2$  to match the data resolution of  $\sim 4$  MeV/ $c^2$ . The  $M_{bc}$  resolution in the  $D^+ \rightarrow K_S^0 e^+ \nu_e$  signal MC matches the data resolution very well so we apply no additional smearing to this mode in the fit.

In summary we have 27 free parameters in the fit: the 20 signal rates, the 4 non-signal  $D\bar{D}$  normalizations and the 3  $M_{bc}$  smearing parameters. This leaves us with a total of  $280 - 27 = 253$  degrees of freedom for the fit.

## C. Checks and Results

The direct fit results are displayed as plots in  $M_{bc}$ , divided into the appropriate  $q^2$  ranges. These are shown in Fig. 1. The value of the likelihood for this fit is  $-2 \ln \mathcal{L} = 275.5$  for 253 degrees of freedom. Note that each of the 20 distributions is described by mainly one free parameter – the signal rate within that bin, with a more constrained contribution from the parameters (resolution and  $D\bar{D}$  background rate) that float independently for each signal mode, with the relative contribution into each  $q^2$  interval fixed within a mode. All other contributions are either explicitly or effectively fixed by other constraints.

Other important reconstructed kinematic variables are presented integrated over  $q^2$  with the components scaled according to the nominal fit. Fig. 2a shows the  $\Delta E$  distributions for events within the signal-enhanced region  $|M_{bc} - M_D| < 0.015$  GeV/ $c^2$ . Fig. 2b shows  $\cos \theta_{W_e}$ , the cosine of the angle between the  $W$  in the  $D$  rest frame and the electron in the  $W$  rest frame, in the signal  $M_{bc}$  and  $\Delta E$  regions. All of our signal modes should exhibit a  $\sin^2 \theta_{W_e}$  dependence independent of the form factor though acceptance effects distort the reconstructed distribution. The fits describe the observed distributions very well. Finally we find that our fit generally agrees well with the observed momentum ( $p_e$ ) spectrum for the signal electron (Fig. 2c). The poorest agreement is exhibited by the  $\pi^0 e \nu_e$  mode, where the probability of  $\chi^2$

3600907-020

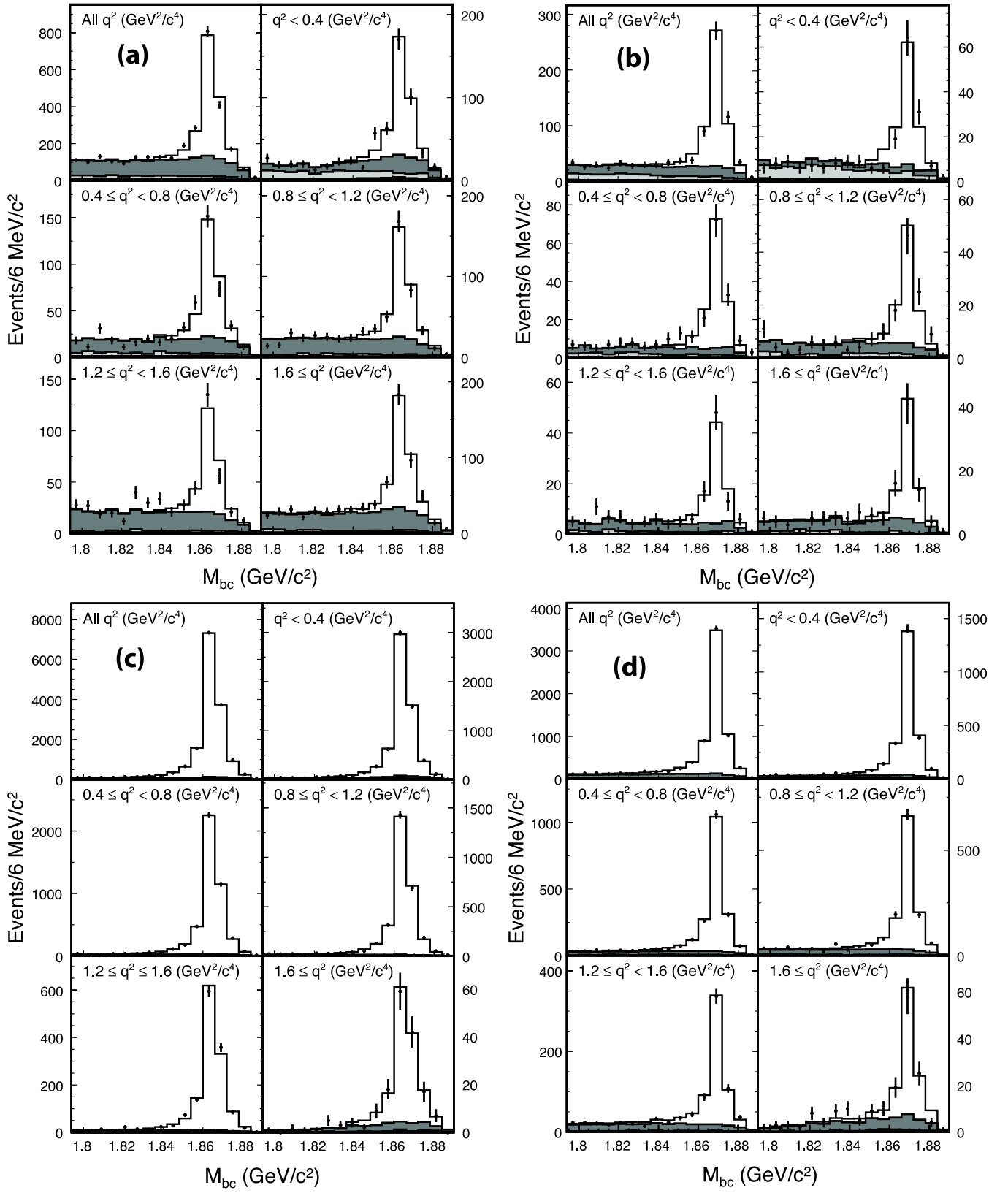


FIG. 1:  $M_{bc}$  distributions for the modes (a)  $D^0 \rightarrow \pi^- e^+ \nu_e$ , (b)  $D^+ \rightarrow \pi^0 e^+ \nu_e$ , (c)  $D^0 \rightarrow K^- e^+ \nu_e$ , and (d)  $D^+ \rightarrow K_S^0 e^+ \nu_e$ . The data are shown by the points, and the fit components (histograms) are normalized using the nominal fit results (see text): signal MC (clear), cross-feed and non-signal  $D\bar{D}$  MC (gray), continuum MC (light gray) and  $e^+$  fakes (black).



TABLE I: Results of fit to  $D\bar{D}$  MC sample with statistics of  $40 \times \mathcal{L}_{\text{data}}$  for all  $q^2$  bins.  $Y_{\text{input}}$  is the true yield,  $Y_{\text{fit}}$  the efficiency corrected yield from the fit, and  $\sigma_{Y_{\text{fit}}}$  the  $1\sigma$  error on the efficiency-corrected fit yield.

| Decay             | $(Y_{\text{input}} - Y_{\text{fit}})/\sigma_{Y_{\text{fit}}}$ |           |           |           |            | All $q^2$ |
|-------------------|---|-----------|-----------|-----------|------------|-----------|
|                   | True $q^2$ interval ( $\text{GeV}^2/c^4$ )                    |           |           |           |            |           |
|                   | < 0.4   | 0.4 – 0.8 | 0.8 – 1.2 | 1.2 – 1.6 | $\geq 1.6$ |           |
| $\pi^- e^+ \nu_e$ | 0.55  | -0.92     | 0.98      | -0.33     | 1.16       | 0.51      |
| $\pi^0 e^+ \nu_e$ | -1.57   | 0.37      | -0.55     | 0.85      | 0.98       | -0.95     |
| $K^- e^+ \nu_e$   | -2.34   | 1.27      | 1.54      | 0.18      | 0.99       | -0.14     |
| $K_S^0 e^+ \nu_e$ | -0.29   | -0.49     | 1.77      | 1.14      | 0.54       | 0.76      |

is still over 3%.

To test the fitting procedure, we fit a set of mock data with known input branching fractions created from the large  $D\bar{D}$  MC sample ( $\sim 40 \times \mathcal{L}_{\text{data}}$ ) used to obtain our non-signal  $D\bar{D}$  background estimate. We fit the sample using distributions from our standard signal MC and from the non-signal portion of the generic  $D\bar{D}$  sample. Because our “data” in this case derives from the same underlying decay model and detector simulation as our fit inputs, we do not apply the corrections noted in the previous section that remove data/MC differences.

Table I presents the differences between our measured and the generator-level rates. We see no biases at this greater level of sensitivity, demonstrating the reliability of the fitting procedure. Furthermore, the semileptonic modes in the generic MC sample used to simulate the “data” were generated using ISGW2 [29] form factors, which have a significantly different  $q^2$  behavior than the LQCD-derived form factors [2] of our signal MC. Our test therefore also verifies that we have adequately subdivided the  $q^2$  range to avoid significant dependence on input form factor modeling, even at levels significantly more sensitive than we can probe with the current data.

## V. EXPERIMENTAL SYSTEMATIC UNCERTAINTIES

The systematic uncertainties for the  $D^0$  modes are summarized in Tables II and III. The first table presents the complete list, while the second breaks down the neutrino-reconstruction simulation errors into component parts. The corresponding systematics tables for the  $D^+$  modes are presented in Tables IV and V. For individual uncertainties we give the sign of the error relative to the change in the lowest  $q^2$  range. The largest systematic uncertainties are those associated with the number of  $D\bar{D}$  pairs (needed for normalization in the branching fraction determination, as described in Section VI) and with neutrino reconstruction simulation. Uncertainties in neutrino simulation include both inaccuracies in detector simulation and uncertainty in the decay model of the non-signal  $D$ , as discussed above.

The starting point for the assessment of many of the

systematic uncertainties is the measurement of any discrepancies between data and MC in the desired quantities (e.g., signal pion efficiency, signal kaon efficiency, etc.). Such measurements (or limits) are made using an independent data sample - in most cases, a sample of events with one of the two  $D$  mesons from the  $\psi(3770)$  fully reconstructed in a hadronic mode. In the case of significant discrepancies, the MC samples are corrected for use in our nominal fit (the fit used to obtain our final branching fraction results, as opposed to any of the fits used to obtain systematic uncertainties) as noted above. Such corrections lead to changes in the measured yields of up to a few percent, but are determined precisely enough to yield sub-percent systematic uncertainties. For each systematic category, we determine the size of its contribution by biasing the MC samples away from their nominal configuration at the level given by the uncertainty of the independent study. We re-fit the data with these biased MC samples, and use the deviation of the fit results from their nominal values to provide an estimate of the uncertainty. We note that because of the correlations among the five  $q^2$  intervals in a given mode, the sum over  $q^2$  of the systematic errors tends to be less sensitive to the systematic variations than the individual intervals themselves.

The number of  $D\bar{D}$  pairs, used to convert the measured yields to branching fractions (see below), is a direct product of the CLEO-c hadronic branching fraction analysis [30]. We combine the statistical and systematic uncertainties from that analysis for our uncertainty estimates.

We have assessed the uncertainties associated with the finding and identification efficiency for each of the signal hadrons. For the signal  $K^\pm$  and  $\pi^\pm$ , the charged track-finding efficiency is already accounted in the tracking efficiency portion of the  $\nu$  simulation uncertainty. They have, however, additional particle identification (PID) criteria associated with them, for which we assess a correction and uncertainty. For the signal  $\pi^0$  and  $K_S^0$  we assess a correction and uncertainty for the reconstruction efficiencies of these particles. We evaluate each of these four uncertainties by first measuring a momentum dependent, and hence  $q^2$  dependent, correction and fit the measurements with a linear parameterization. The best fit result is applied as a correction in the nominal fit. To evaluate the systematic uncertainty, we identify the largest systematic variation on the  $\chi^2 = 1$  ellipse from the linear fit. The branching fractions are most affected by the largest variation in overall normalization, while the form factors (Section VII) are most affected by the largest variation in slope.

We have uncertainties associated with the electron identification efficiency and the rates for hadrons to misreconstruct as (fake) electrons. We vary the efficiency and fake rates used in the analysis of our MC samples (see Section IV B) according to the uncertainties from the data studies used to measure them, and re-fit the data to evaluate our sensitivity.

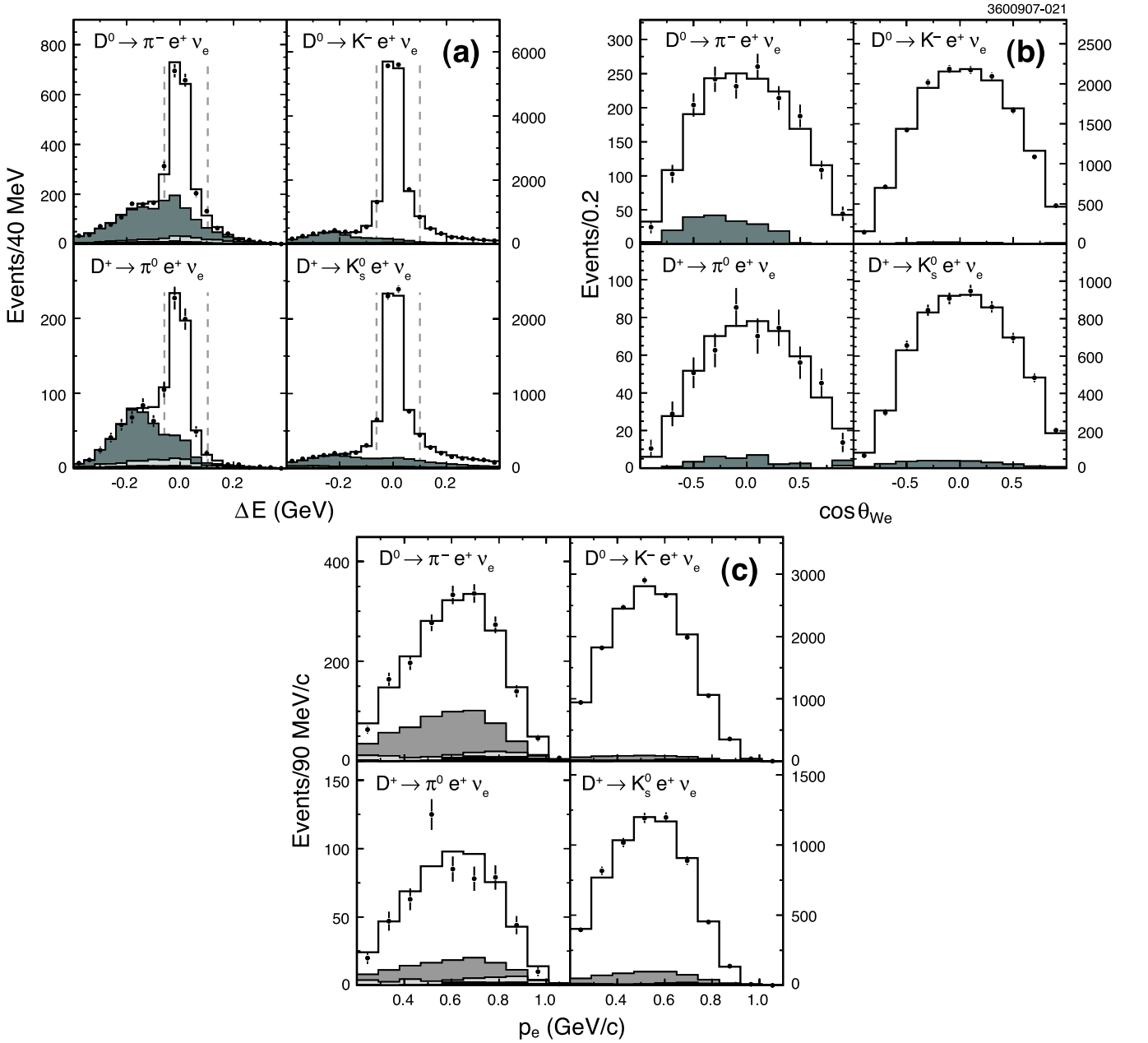


FIG. 2: The kinematic distributions for (a)  $\Delta E$ , (b)  $\cos\theta_{We}$ , and (c)  $p_e$ , for events falling within the  $M_{bc}$  signal region for each of the four signal modes. The data are shown by the points, and the fit components (histograms) are normalized using the nominal fit results (see text): signal MC (clear), cross-feed and non-signal  $D\bar{D}$  MC (gray), continuum MC (light gray) and  $e^+$  fakes (black). The dotted lines in (a) indicate for each mode the  $\Delta E$  region used in fitting.

Modeling of  $\pi^\pm$  and  $\pi^0$  production – spectra and rates – in  $D$  decay significantly affects the background shape and rate for the signal cross-feed background into the pion signal modes. The large effect results because a pion from the non-signal  $D$  decay can be swapped in as the signal pion candidate. We measure the background pion spectra in data using the inclusive  $D$  decays on the “other side” of a fully reconstructed hadronically-decayed  $D$  “tag”, and correct the MC spectra accordingly. To be conservative in the associated systematic

uncertainty, we take the full difference for results obtained using corrected and uncorrected spectra. In the signal  $D^0 \rightarrow \pi^- e^+ \nu_e$  mode we also correct the cross-feed background from  $D^0 \rightarrow K^- e^+ \nu_e$  events that results from misidentifying a  $K^\pm$  as a  $\pi^\pm$ . Once again the uncertainty estimate is taken as the difference of our measured rates obtained using the corrected and uncorrected fake rates.

For three of our signal modes,  $D^0 \rightarrow \pi^- e^+ \nu_e$ ,  $D^0 \rightarrow K^- e^+ \nu_e$  and  $D^+ \rightarrow \pi^0 e^+ \nu_e$ , we have systematic uncertainty associated with the additional  $M_{bc}$  resolution pa-

TABLE II: Summary of full and partial branching fraction systematic errors (%) for the  $D^0 \rightarrow \pi^- e^+ \nu_e$  and  $D^0 \rightarrow K^- e^+ \nu_e$  signal decay modes. The sign represents the direction of change relative to the change in the  $[0, 0.4)$  GeV $^2/c^4$  interval in each mode.

|                                 | $D^0 \rightarrow \pi^- e^+ \nu_e$ |            |            |            |                      |           | $D^0 \rightarrow K^- e^+ \nu_e$ |            |            |            |                      |           |
|---------------------------------|-----------------------------------|------------|------------|------------|----------------------|-----------|---------------------------------|------------|------------|------------|----------------------|-----------|
|                                 | $q^2$ interval (GeV $^2/c^4$ )    |            |            |            |                      |           | $q^2$ interval (GeV $^2/c^4$ )  |            |            |            |                      |           |
| Systematic                      | [0, 0.4)                          | [0.4, 0.8) | [0.8, 1.2) | [1.2, 1.6) | [1.6, $q_{\max}^2$ ] | All $q^2$ | [0, 0.4)                        | [0.4, 0.8) | [0.8, 1.2) | [1.2, 1.6) | [1.6, $q_{\max}^2$ ] | All $q^2$ |
| Number $D\bar{D}$               | 1.51                              | 1.51       | 1.51       | 1.51       | 1.51                 | 1.51      | 1.51                            | 1.51       | 1.51       | 1.51       | 1.51                 | 1.51      |
| $\nu_e$ simulation              | 1.45                              | 1.77       | 2.21       | 2.87       | 1.59                 | 1.69      | 1.52                            | 1.99       | 1.96       | 2.39       | 1.28                 | 1.80      |
| $\pi^0$ efficiency              | 0.01                              | 0.01       | 0.01       | 0.00       | -0.03                | -0.00     | 0.00                            | 0.00       | 0.00       | 0.00       | 0.01                 | 0.00      |
| $K_S^0$ efficiency              | 0.01                              | -0.01      | -0.02      | -0.04      | -0.08                | -0.03     | 0.01                            | 0.00       | 0.00       | 0.00       | 0.07                 | 0.01      |
| $\pi^-$ PID                     | 0.44                              | 0.41       | 0.39       | 0.39       | 0.40                 | 0.41      | 0.00                            | 0.00       | 0.00       | 0.00       | 0.00                 | 0.00      |
| $K^-$ PID                       | 0.05                              | 0.02       | 0.02       | 0.01       | 0.02                 | 0.03      | 0.32                            | 0.30       | 0.28       | 0.26       | 0.26                 | 0.30      |
| $e^+$ PID                       | 0.76                              | 0.40       | 0.75       | 0.36       | 0.44                 | 0.56      | 0.65                            | 0.58       | 0.60       | 0.52       | 0.46                 | 0.61      |
| $e^+$ Fakes                     | 2.50                              | 0.45       | -0.01      | 0.05       | 0.92                 | 0.88      | 0.57                            | 0.07       | -0.04      | 0.01       | 0.39                 | 0.25      |
| $\pi^0$ production              | 0.01                              | 0.02       | 0.03       | 0.01       | 0.06                 | 0.03      | 0.00                            | 0.00       | -0.01      | 0.00       | 0.01                 | 0.00      |
| $\pi^-$ production              | 0.07                              | 0.42       | 0.44       | 0.10       | -1.96                | -0.24     | 0.00                            | 0.00       | 0.00       | 0.05       | 0.23                 | 0.01      |
| $K^-$ fakes                     | 0.67                              | 1.01       | 0.93       | 0.35       | -0.08                | 0.58      | 0.00                            | 0.00       | -0.01      | -0.01      | -0.02                | 0.00      |
| $\pi^- e^+ \nu_e$ $M_{bc}$ res. | 0.93                              | 1.06       | 0.85       | 0.83       | 1.05                 | 0.95      | 0.02                            | 0.01       | 0.01       | 0.01       | 0.06                 | 0.01      |
| $K^- e^+ \nu_e$ $M_{bc}$ res.   | 0.07                              | 0.04       | 0.02       | 0.01       | 0.01                 | 0.03      | 0.09                            | 0.08       | 0.07       | 0.09       | 0.16                 | 0.09      |
| $\pi^0 e^+ \nu_e$ $M_{bc}$ res. | 0.01                              | 0.02       | 0.00       | 0.01       | -0.13                | -0.02     | 0.00                            | 0.00       | 0.00       | 0.00       | 0.00                 | 0.00      |
| $e^+$ veto                      | 0.05                              | 0.04       | -0.01      | -0.14      | -0.01                | 0.00      | 0.08                            | 0.07       | 0.00       | -0.02      | -0.03                | 0.05      |
| FSR                             | 0.85                              | 1.53       | 0.97       | 0.91       | 0.75                 | 0.99      | 0.63                            | 0.61       | 0.56       | 0.48       | 0.47                 | 0.59      |
| Model dep.                      | 0.50                              | -0.01      | -0.09      | 0.43       | -1.55                | -0.19     | 0.33                            | -0.11      | -0.16      | -0.41      | -1.29                | 0.02      |
| <b>Total</b>                    | 3.70                              | 3.26       | 3.26       | 3.56       | 3.74                 | 2.95      | 2.44                            | 2.66       | 2.63       | 2.95       | 2.51                 | 2.53      |

TABLE III: Summary of full and partial branching fraction systematic errors (%) associated with neutrino modeling in the MC for the  $D^0 \rightarrow \pi^- e^+ \nu_e$  and  $D^0 \rightarrow K^- e^+ \nu_e$  signal decay modes. The sign represents the direction of change relative to the change in the  $[0, 0.4)$  GeV $^2/c^4$  interval in each mode.

|                     | $D^0 \rightarrow \pi^- e^+ \nu_e$ |            |            |            |                      |           | $D^0 \rightarrow K^- e^+ \nu_e$ |            |            |            |                      |           |
|---------------------|-----------------------------------|------------|------------|------------|----------------------|-----------|---------------------------------|------------|------------|------------|----------------------|-----------|
|                     | $q^2$ interval (GeV $^2/c^4$ )    |            |            |            |                      |           | $q^2$ interval (GeV $^2/c^4$ )  |            |            |            |                      |           |
| $\nu$ Systematic    | [0, 0.4)                          | [0.4, 0.8) | [0.8, 1.2) | [1.2, 1.6) | [1.6, $q_{\max}^2$ ] | All $q^2$ | [0, 0.4)                        | [0.4, 0.8) | [0.8, 1.2) | [1.2, 1.6) | [1.6, $q_{\max}^2$ ] | All $q^2$ |
| split-off showers   | 0.58                              | 0.90       | 1.92       | 2.58       | 0.48                 | 1.17      | 0.89                            | 1.54       | 1.49       | 2.00       | 0.67                 | 1.29      |
| $K_L^0$ showers     | 0.15                              | 0.13       | 0.11       | 0.06       | -0.60                | -0.04     | 0.01                            | -0.02      | -0.04      | -0.05      | -0.06                | -0.01     |
| $K_L^0$ production  | 0.67                              | 0.66       | 0.66       | 0.67       | 0.65                 | 0.66      | 0.66                            | 0.65       | 0.66       | 0.67       | 0.69                 | 0.66      |
| track efficiency    | 0.60                              | 0.56       | 0.50       | 0.63       | 0.45                 | 0.54      | 0.37                            | 0.39       | 0.44       | 0.44       | 0.21                 | 0.39      |
| track resolution    | 0.00                              | 1.02       | 0.01       | 0.46       | 0.85                 | 0.46      | 0.28                            | 0.43       | 0.50       | 0.60       | 0.34                 | 0.39      |
| split-off rejection | 0.58                              | -0.02      | 0.16       | 0.04       | -0.22                | 0.12      | 0.59                            | 0.56       | 0.48       | 0.43       | 0.21                 | 0.54      |
| particle ID         | 0.01                              | -0.02      | 0.08       | 0.02       | 0.09                 | 0.04      | 0.06                            | 0.04       | 0.05       | 0.03       | 0.04                 | 0.05      |
| shower resolution   | 0.03                              | 0.09       | 0.06       | -0.01      | 0.11                 | 0.06      | 0.00                            | 0.00       | 0.00       | 0.00       | -0.01                | 0.00      |
| fake tracks         | 0.76                              | 0.71       | 0.70       | 0.71       | 0.72                 | 0.72      | 0.72                            | 0.72       | 0.71       | 0.71       | 0.71                 | 0.72      |
| <b>Total</b>        | 1.45                              | 1.77       | 2.21       | 2.87       | 1.59                 | 1.69      | 1.52                            | 1.99       | 1.96       | 2.39       | 1.28                 | 1.80      |

parameter. The statistical uncertainty already has a contribution from allowing this parameter to float. We estimate the contribution to the systematic uncertainty for each mode by increasing the value of that mode's resolution parameter by one standard deviation beyond the best fit result.

We must also account for any uncertainty associated with modeling event loss from the single electron veto because of secondary electrons from photon conversions and other processes. According to data studies (using the CLEO-c “tagged” samples, where one of the two  $D$  mesons from the  $\psi(3770)$  is fully reconstructed), our MC simulation models the number of secondary electrons in our events accurately within the error of the study. The

most likely potential source of uncertainty arises from mis-modeling the rate for photon conversion within the detector material. For the uncertainty estimate we therefore vary this contribution over the range allowed by the maximum allowed uncertainty of our data study, about 8%.

For the systematic uncertainty associated with the final state radiation (FSR) modeling, we take the difference between the KLOR and PHOTOS predictions. This simulates a change in the radiative branching fraction of up to 16% in the most extreme case. Because the majority of the correction results from the lack of the FSR interference terms between the charged hadron and electron, the systematic should be an overestimate of

TABLE IV: Summary of full and partial branching fraction systematic errors (%) for the  $D^+ \rightarrow \pi^0 e^+ \nu_e$  and  $D^+ \rightarrow \bar{K}^0 e^+ \nu_e$  signal decay modes. The sign represents the direction of change relative to the change in the  $[0, 0.4)$  GeV $^2/c^4$  interval in each mode.

|                                 | $D^+ \rightarrow \pi^0 e^+ \nu_e$ |            |            |            |                      |           | $D^+ \rightarrow \bar{K}^0 e^+ \nu_e$ |            |            |            |                      |           |
|---------------------------------|-----------------------------------|------------|------------|------------|----------------------|-----------|---------------------------------------|------------|------------|------------|----------------------|-----------|
|                                 | $q^2$ interval (GeV $^2/c^4$ )    |            |            |            |                      |           | $q^2$ interval (GeV $^2/c^4$ )        |            |            |            |                      |           |
| Systematic                      | [0, 0.4)                          | [0.4, 0.8) | [0.8, 1.2) | [1.2, 1.6) | [1.6, $q_{\max}^2$ ] | All $q^2$ | [0, 0.4)                              | [0.4, 0.8) | [0.8, 1.2) | [1.2, 1.6) | [1.6, $q_{\max}^2$ ] | All $q^2$ |
| Number $D\bar{D}$               | 1.60                              | 1.60       | 1.60       | 1.60       | 1.60                 | 1.60      | 1.60                                  | 1.60       | 1.60       | 1.60       | 1.60                 | 1.60      |
| $\nu$ simulation                | 2.54                              | 3.41       | 2.57       | 2.53       | 2.45                 | 1.96      | 1.71                                  | 1.75       | 1.82       | 1.84       | 2.18                 | 1.74      |
| $\pi^0$ efficiency              | 0.87                              | 0.56       | 0.77       | 1.07       | 1.07                 | 0.85      | 0.00                                  | 0.01       | -0.01      | -0.02      | 0.00                 | 0.00      |
| $K_S^0$ efficiency              | 0.02                              | 0.02       | 0.08       | 0.11       | 0.18                 | 0.07      | 1.05                                  | 1.00       | 0.94       | 0.88       | 0.81                 | 1.00      |
| $\pi^-$ PID                     | 0.17                              | 0.37       | 0.13       | -0.24      | -0.29                | 0.06      | 0.01                                  | 0.01       | 0.00       | -0.03      | -0.02                | 0.00      |
| $K^-$ PID                       | 0.17                              | 0.37       | 0.12       | -0.24      | -0.29                | 0.06      | 0.01                                  | 0.01       | 0.00       | -0.02      | 0.00                 | 0.00      |
| $e^+$ PID                       | 1.13                              | 0.56       | 0.33       | 0.98       | 0.01                 | 0.62      | 0.62                                  | 0.65       | 0.52       | 0.59       | 0.76                 | 0.61      |
| $e^+$ Fakes                     | 1.52                              | 0.14       | -0.29      | -0.07      | 0.64                 | 0.44      | 0.38                                  | -0.03      | -0.17      | 0.09       | 1.00                 | 0.14      |
| $\pi^0$ production              | 0.43                              | 0.81       | 0.76       | -0.73      | -1.87                | -0.04     | 0.02                                  | -0.01      | 0.00       | -0.11      | -0.14                | -0.01     |
| $\pi^-$ production              | 0.07                              | -0.02      | 0.03       | 0.02       | 1.46                 | 0.29      | 0.02                                  | -0.01      | 0.00       | 0.19       | 1.12                 | 0.04      |
| $K^-$ fakes                     | 0.01                              | -0.01      | 0.04       | 0.07       | 0.20                 | 0.05      | 0.01                                  | 0.01       | -0.03      | -0.07      | -0.16                | -0.01     |
| $\pi^- e^+ \nu_e$ $M_{bc}$ res. | 0.00                              | 0.00       | -0.01      | 0.05       | -0.29                | -0.05     | 0.01                                  | 0.01       | 0.00       | 0.04       | 0.09                 | 0.01      |
| $K^- e^+ \nu_e$ $M_{bc}$ res.   | 0.00                              | 0.01       | 0.00       | 0.00       | 0.01                 | 0.00      | 0.02                                  | 0.01       | 0.00       | 0.00       | 0.02                 | 0.01      |
| $\pi^0 e^+ \nu_e$ $M_{bc}$ res. | 2.62                              | 1.27       | 3.77       | 1.17       | 1.97                 | 2.09      | 0.01                                  | 0.01       | 0.01       | 0.05       | 0.08                 | 0.01      |
| $e^+$ veto                      | 0.26                              | -0.01      | 0.20       | 0.03       | -0.14                | 0.07      | 0.02                                  | 0.09       | 0.02       | 0.12       | -0.30                | 0.04      |
| FSR                             | 0.26                              | 0.48       | 0.47       | 0.68       | 0.65                 | 0.49      | 0.25                                  | 0.46       | 0.55       | 0.64       | 0.60                 | 0.41      |
| Model dep.                      | 0.56                              | 0.08       | -0.08      | 0.76       | 0.08                 | 0.28      | 0.35                                  | -0.16      | -0.28      | -0.83      | -1.51                | -0.06     |
| <b>Total</b>                    | 4.57                              | 4.19       | 5.00       | 3.76       | 4.52                 | 3.53      | 2.70                                  | 2.70       | 2.73       | 2.87       | 3.69                 | 2.67      |

TABLE V: Summary of full and partial branching fraction systematic errors (%) associated with neutrino modeling in the MC for the  $D^+ \rightarrow \pi^0 e^+ \nu_e$  and  $D^+ \rightarrow \bar{K}^0 e^+ \nu_e$  signal decay modes. The sign represents the direction of change relative to the change in the  $[0, 0.4)$  GeV $^2/c^4$  interval in each mode.

|                     | $D^+ \rightarrow \pi^0 e^+ \nu_e$ |            |            |            |                      |           | $D^+ \rightarrow \bar{K}^0 e^+ \nu_e$ |            |            |            |                      |           |
|---------------------|-----------------------------------|------------|------------|------------|----------------------|-----------|---------------------------------------|------------|------------|------------|----------------------|-----------|
|                     | $q^2$ interval (GeV $^2/c^4$ )    |            |            |            |                      |           | $q^2$ interval (GeV $^2/c^4$ )        |            |            |            |                      |           |
| $\nu$ Systematic    | [0, 0.4)                          | [0.4, 0.8) | [0.8, 1.2) | [1.2, 1.6) | [1.6, $q_{\max}^2$ ] | All $q^2$ | [0, 0.4)                              | [0.4, 0.8) | [0.8, 1.2) | [1.2, 1.6) | [1.6, $q_{\max}^2$ ] | All $q^2$ |
| split-off showers   | 0.62                              | 2.94       | 2.11       | 1.30       | -1.68                | 1.14      | 0.17                                  | 0.37       | 0.21       | -0.13      | -1.36                | 0.18      |
| $K_L^0$ showers     | 0.19                              | 0.17       | 0.08       | 0.13       | -0.83                | -0.03     | 0.01                                  | 0.06       | -0.08      | -0.15      | -0.46                | -0.02     |
| $K_L^0$ production  | 1.10                              | 1.07       | 1.07       | 1.08       | 1.13                 | 1.09      | 1.07                                  | 1.07       | 1.09       | 1.10       | 1.09                 | 1.08      |
| track efficiency    | 0.51                              | 0.37       | 0.18       | -0.14      | 0.13                 | 0.24      | 0.62                                  | 0.57       | 0.70       | 0.66       | 0.39                 | 0.62      |
| track resolution    | 1.08                              | 0.05       | -0.09      | -0.90      | 0.13                 | 0.12      | 0.43                                  | 0.45       | 0.64       | 0.49       | 0.92                 | 0.49      |
| split-off rejection | 1.66                              | 1.08       | 0.68       | 1.45       | -0.81                | 0.86      | 0.81                                  | 0.88       | 0.84       | 0.99       | 0.21                 | 0.84      |
| particle ID         | 0.09                              | -0.02      | 0.04       | 0.07       | -0.03                | 0.03      | 0.01                                  | 0.02       | 0.00       | 0.01       | 0.08                 | 0.01      |
| shower resolution   | 0.00                              | -0.01      | 0.18       | 0.30       | 0.04                 | 0.08      | 0.00                                  | -0.02      | 0.03       | -0.01      | -0.09                | 0.00      |
| fake tracks         | 0.77                              | 0.71       | 0.70       | 0.71       | 0.71                 | 0.72      | 0.72                                  | 0.70       | 0.69       | 0.69       | 0.70                 | 0.71      |
| <b>Total</b>        | 2.54                              | 3.41       | 2.57       | 2.53       | 2.45                 | 1.96      | 1.71                                  | 1.75       | 1.82       | 1.84       | 2.18                 | 1.74      |

the FSR uncertainty from final or initial-state particles. This overestimate compensates for the unknown direct (structure-dependent) contributions.

The final systematic error we assess is the dependence on our modeling of the form factor input to our signal MC. We reweight each of our signal MC samples with a different form factor input, namely ISGW2. The nominal form factor input to our signal MC is a BK parameterization [8] with parameters determined by lattice QCD [2]. The  $q^2$  spectra of the latter differ markedly from those of ISGW2. We fit with the re-weighted MC spectra and the difference to the nominal fit gives the systematic error associated with model dependence. The small uncertainties obtained in this study confirm our conclusion drawn

from fitting the large MC sample.

## VI. BRANCHING FRACTION RESULTS

Combining the results of the fit and the systematic uncertainty estimates gives us the final efficiency-corrected yield measurement for each mode. From that yield ( $Y$ ), we obtain the branching fraction  $\mathcal{B} = Y/2N_{D\bar{D}}$ , where  $N_{D\bar{D}}$  is the number of neutral ( $N_{D^0\bar{D}^0}$ ) or charged ( $N_{D^+\bar{D}^-}$ ) pairs in our sample. We obtain these numbers from an independent CLEO-c analysis [30] based on the comparison of events with one reconstructed  $D$  to events with both  $D$  decays reconstructed, in certain

TABLE VI: Summary of the efficiencies ( $\varepsilon$ ) and efficiency-corrected yields for each  $q^2$  interval and the corresponding partial branching fractions, the total branching fractions, the branching ratios and the isospin ratios. In all cases the first errors are statistical and the second are systematic. For the  $\bar{K}^0$  mode, the efficiency and yields correspond to the reconstructed  $K_S^0 \rightarrow \pi^+\pi^-$  mode, so do not include the initial production amplitude or  $\pi^+\pi^-$  branching fraction factors.

|  | $q^2$ interval ( $\text{GeV}^2/c^4$ ) |                 |                 |                |               | Total         |
|--|---------------------------------------|-----------------|-----------------|----------------|---------------|---------------|
|  | $< 0.4$                               | $0.4 - 0.8$     | $0.8 - 1.2$     | $1.2 - 1.6$    | $\geq 1.6$    |               |
|  | $D^0 \rightarrow \pi^- e^+ \nu_e$     |                 |                 |                |               |               |
| $\varepsilon$ (%)                      | 19.4                                  | 21.0            | 22.4            | 22.8           | 22.4          | –             |
| Yield                                  | 1452(113)(49)                         | 1208(102)(35)   | 1242(99)(36)    | 906(85)(29)    | 1357(103)(46) | –             |
| $\mathcal{B}(\pi^- e^+ \nu_e)$ (%)     | 0.070(5)(3)                           | 0.059(5)(2)     | 0.060(5)(2)     | 0.044(4)(2)    | 0.066(5)(2)   | 0.299(11)(9)  |
|  | $D^+ \rightarrow \pi^0 e^+ \nu_e$     |                 |                 |                |               |               |
| $\varepsilon$ (%)                      | 7.5                                   | 8.0             | 7.9             | 7.2            | 5.7           | –             |
| Yield                                  | 1379(168)(59)                         | 1584(180)(61)   | 1012(154)(48)   | 1028(158)(35)  | 1101(174)(47) | –             |
| $\mathcal{B}(\pi^0 e^+ \nu_e)$ (%)     | 0.084(10)(4)                          | 0.097(11)(4)    | 0.062(9)(3)     | 0.063(10)(2)   | 0.067(11)(3)  | 0.373(22)(13) |
|  | $D^0 \rightarrow K^- e^+ \nu_e$       |                 |                 |                |               |               |
| $\varepsilon$ (%)                      | 19.2                                  | 20.5            | 20.0            | 18.3           | 13.9          | –             |
| Yield                                  | 29701(441)(569)                       | 21600(377)(473) | 14032(304)(301) | 7001(225)(178) | 991(112)(20)  | –             |
| $\mathcal{B}(K^- e^+ \nu_e)$ (%)       | 1.441(21)(35)                         | 1.048(18)(28)   | 0.681(15)(18)   | 0.340(11)(10)  | 0.048(5)(12)  | 3.557(33)(90) |
|  | $D^+ \rightarrow \bar{K}^0 e^+ \nu_e$ |                 |                 |                |               |               |
| $\varepsilon$ (%)                      | 11.7                                  | 12.3            | 12.5            | 12.2           | 12.5          | –             |
| Yield                                  | 19480(466)(417)                       | 14422(415)(306) | 9009(327)(194)  | 4656(236)(107) | 789(104)(26)  | –             |
| $\mathcal{B}(\bar{K}^0 e^+ \nu_e)$ (%) | 3.436(82)(93)                         | 2.544(73)(69)   | 1.589(58)(44)   | 0.821(42)(24)  | 0.139(18)(5)  | 8.53(13)(23)  |
| $R_0$ (%)                              | 4.89(39)(12)                          | 5.59(48)(12)    | 8.85(74)(15)    | 12.9(13)(2)    | 137(19)(3)    | 8.41(32)(13)  |
| $R_+$ (%)                              | 2.45(31)(9)                           | 3.80(45)(13)    | 3.89(61)(17)    | 7.6(12)(2)     | 48(10)(2)     | 4.37(27)(12)  |
| $I_\pi$                                | 2.12(31)(9)                           | 1.54(22)(7)     | 2.47(43)(13)    | 1.78(32)(7)    | 2.48(45)(13)  | 2.03(14)(8)   |
| $I_K$                                  | 1.06(3)(3)                            | 1.04(4)(3)      | 1.09(5)(3)      | 1.05(6)(4)     | 0.88(15)(3)   | 1.06(2)(3)    |

hadronic modes. For the same data set that we have used, that analysis finds  $N_{D^0 \bar{D}^0} = (1.031 \pm 0.016) \times 10^6$  and  $N_{D^+ D^-} = (0.819 \pm 0.013) \times 10^6$ . Our fit yields, efficiencies and branching fractions for each mode, in each  $q^2$  range, are presented in Table VI. The total branching fractions for each mode (also listed in Table VI) are

$$\mathcal{B}(D^0 \rightarrow \pi^- e^+ \nu_e) = 0.299(11)(9)\%, \quad (14)$$

$$\mathcal{B}(D^+ \rightarrow \pi^0 e^+ \nu_e) = 0.373(22)(13)\%, \quad (15)$$

$$\mathcal{B}(D^0 \rightarrow K^- e^+ \nu_e) = 3.56(3)(9)\%, \quad (16)$$

and

$$\mathcal{B}(D^+ \rightarrow \bar{K}^0 e^+ \nu_e) = 8.53(13)(23)\%. \quad (17)$$

The errors listed are statistical and systematic, respectively.

We also measure the branching fraction and partial width ratios in each  $q^2$  range. The full results are given in Table VI. To determine the partial width ratios we used the Particle Data Group lifetimes [4]  $\tau_{D^0} = 410.3 \pm 1.5$  fs and  $\tau_{D^+} = 1040 \pm 7$  fs. For the integrated  $q^2$  ranges we find the ratios of branching fractions

$$R_0 \equiv \frac{\mathcal{B}(D^0 \rightarrow \pi^- e^+ \nu_e)}{\mathcal{B}(D^0 \rightarrow K^- e^+ \nu_e)} = 8.41(32)(13)\% \quad (18)$$

and

$$R_+ \equiv \frac{\mathcal{B}(D^+ \rightarrow \pi^0 e^+ \nu_e)}{\mathcal{B}(D^+ \rightarrow \bar{K}^0 e^+ \nu_e)} = 4.37(27)(12)\%. \quad (19)$$

The partial width ratios, which are expected to satisfy isospin relationships, are found to be

$$I_\pi \equiv \frac{\Gamma(D^0 \rightarrow \pi^- e^+ \nu_e)}{\Gamma(D^+ \rightarrow \pi^0 e^+ \nu_e)} = 2.03(14)(8) \quad (20)$$

and

$$I_K \equiv \frac{\Gamma(D^0 \rightarrow K^- e^+ \nu_e)}{\Gamma(D^+ \rightarrow \bar{K}^0 e^+ \nu_e)} = 1.06(2)(3). \quad (21)$$

We expect  $I_\pi = 2$  and  $I_K = 1$ , hence the measured partial width ratios satisfy isospin symmetry within our experimental precision.

## VII. FORM FACTORS

For each of our four signal decay modes we have obtained partial branching fraction results in five  $q^2$  ranges. To extract information about the form factors we use the relationship

$$\mathcal{B}_i = \frac{G_F^2 |V_{cq}|^2}{24\pi^3 \Gamma_D} \int_{q_{\min}^2}^{q_{\max}^2} p^3 |f_+(q^2)|^2 dq^2 \quad (22)$$

TABLE VII: Summary of form factor results for the series parameterization and pole model fits. Correlation coefficients for the total uncertainty between variables in any two (three) preceding columns are given by  $\rho$  ( $\rho_{ij}$ ). The first errors are statistical and the second are systematic. The values for the  $\pi^0 e^+ \nu_e$  mode are isospin corrected. For the series parameters ( $a_i$ ) we have assumed  $|V_{cs}| = 0.976$  and  $|V_{cd}| = 0.224$ .

| Series Parameterization - Three Parameter Fits |                  |                                 |               |                  |                          |             |                  |                        |        |                |
|--|------------------|---------------------------------|---------------|------------------|--------------------------|-------------|------------------|------------------------|--------|----------------|
| Decay  | $a_0$            | $a_1$                           | $a_2$         | $\rho_{01}$      | $\rho_{02}$              | $\rho_{12}$ | $ V_{cq} f_+(0)$ | $1 + 1/\beta - \delta$ | $\rho$ | $\chi^2/d.o.f$ |
| $\pi^- e^+ \nu_e$                              | 0.044(2)(1)      | -0.18(7)(2)                     | -0.03(35)(12) | 0.81             | 0.71                     | 0.96        | 0.140(7)(3)      | 1.30(37)(12)           | -0.85  | 2.0/2          |
| $\pi^0 e^+ \nu_e$                              | 0.044(3)(1)      | -0.23(11)(2)                    | -0.60(57)(15) | 0.80             | 0.67                     | 0.95        | 0.138(11)(4)     | 1.58(60)(13)           | -0.86  | 2.8/2          |
| $K^- e^+ \nu_e$                                | 0.0234(3)(3)     | -0.009(21)(7)                   | 0.52(28)(6)   | 0.62             | 0.56                     | 0.96        | 0.747(9)(9)      | 0.62(13)(4)            | -0.62  | 0.2/2          |
| $\bar{K}^0 e^+ \nu_e$                          | 0.0224(4)(3)     | 0.009(32)(7)                    | 0.76(42)(8)   | 0.72             | 0.64                     | 0.96        | 0.733(14)(11)    | 0.51(20)(4)            | -0.72  | 1.7/2          |
| Series Parameterization - Two Parameter Fits   |                  |                                 |               |                  |                          |             |                  |                        |        |                |
| Decay  | $a_0$            | $a_1$                           | $\rho$        | $ V_{cq} f_+(0)$ | $1 + 1/\beta - \delta$   | $\rho$      | $\chi^2/d.o.f$   |                        |        |                |
| $\pi^- e^+ \nu_e$                              | 0.044(2)(1)      | -0.173(19)(7)                   | 0.66          | 0.140(5)(3)      | 1.27(11)(4)              | -0.80       | 2.0/3            |                        |        |                |
| $\pi^0 e^+ \nu_e$                              | 0.046(2)(1)      | -0.124(30)(9)                   | 0.69          | 0.147(7)(4)      | 1.01(16)(5)              | -0.78       | 4.0/3            |                        |        |                |
| $K^- e^+ \nu_e$                                | 0.0230(2)(3)     | -0.047(6)(3)                    | 0.34          | 0.734(6)(9)      | 0.86(4)(2)               | -0.43       | 3.8/3            |                        |        |                |
| $\bar{K}^0 e^+ \nu_e$                          | 0.0218(3)(3)     | -0.046(9)(4)                    | 0.53          | 0.713(9)(11)     | 0.87(6)(3)               | -0.60       | 4.9/3            |                        |        |                |
| Simple Pole Model Fits                         |                  |                                 |               |                  | Modified Pole Model Fits |             |                  |                        |        |                |
| Decay  | $ V_{cq} f_+(0)$ | $m_{\text{pole}}$ (GeV/ $c^2$ ) | $\rho$        | $\chi^2/d.o.f$   | $ V_{cq} f_+(0)$         | $\alpha$    | $\rho$           | $\chi^2/d.o.f$         |        |                |
| $\pi^- e^+ \nu_e$                              | 0.146(4)(2)      | 1.87(3)(1)                      | 0.63          | 3.11/3           | 0.142(4)(2)              | 0.37(8)(3)  | -0.75            | 2.1/3                  |        |                |
| $\pi^0 e^+ \nu_e$                              | 0.149(6)(3)      | 1.97(7)(2)                      | 0.65          | 4.42/3           | 0.147(7)(4)              | 0.14(16)(4) | -0.75            | 4.07/3                 |        |                |
| $K^- e^+ \nu_e$                                | 0.735(5)(9)      | 1.97(3)(1)                      | 0.36          | 2.67/3           | 0.732(6)(9)              | 0.21(5)(3)  | -0.42            | 4.32/3                 |        |                |
| $\bar{K}^0 e^+ \nu_e$                          | 0.710(8)(10)     | 1.96(4)(2)                      | 0.53          | 4.1/3            | 0.708(9)(10)             | 0.22(8)(3)  | -0.59            | 5.3/3                  |        |                |

to relate the form factor  $f_+(q^2)$  to the partial branching fraction  $\mathcal{B}$  in a particular  $q^2$  range. In this expression,  $\Gamma_D$  is the total decay width of the parent  $D$  meson, and  $i$  denotes the particular  $q^2$  interval. A specific functional form is chosen for  $f_+(q^2)$  (see Section II) and the parameter values are determined via a  $\chi^2$  fit to the five measured  $\mathcal{B}_i$ . In order to account for the correlations between the branching fractions in each  $q^2$  range we minimize the expression

$$\chi^2 = \sum_{ij} (\mathcal{B}_i - y_i) C_{ij}^{-1} (\mathcal{B}_j - y_j), \quad (23)$$

where  $y_i$  is the fit prediction for the branching fraction in the  $i^{\text{th}}$   $q^2$  interval, and  $C_{ij}^{-1}$  is the inverse of the covariance matrix. The integration in each bin is performed numerically on each fit iteration using the trapezoidal rule.

The systematic uncertainties on the form factor parameters are evaluated using the same method as for the branching fraction analysis. We take the set of branching fractions that result from the branching fraction fit for each systematic uncertainty, then redo the fit for the form factors. The difference in these fit parameters from the nominal results is taken as the estimate of the systematic uncertainty. The list of systematic uncertainties evaluated is the same as for the branching fraction analysis (see Section V). Note that for the systematic errors found by exploring a one standard deviation  $\chi^2$  ellipse in normalization versus  $q^2$ -dependence and taking the largest observed deviation from the nominal result ( $\pi^-$  PID,  $K^-$  PID,  $\pi^0$  finding, and  $K_S^0$  finding), the form factors and the branching fractions will have their largest deviations in very different regions of the ellipse. The form factor will be most sensitive to the region of

the ellipse that causes the largest variation as a function of  $q^2$ , while the branching fraction is most sensitive to the overall normalization.

Fitting with the full covariance matrix that includes both statistical and systematic uncertainties and correlations (see Appendix B) yields almost identical central values and total errors.

We evaluate the form factor shape using the functional form given by the series parameterization as described in Section II. For comparative purposes we also provide results based on the two pole models described in Section II. For the series model we perform fits using both the first two and the first three expansion parameters  $a_k$ . This tests both our sensitivity to the number of parameters in the expansion and the convergence of the series. We express our results in terms of the physical observables, the intercept  $|V_{cq}|f_+(0)$  and  $1 + 1/\beta - \delta$ , as well as giving the expansion parameters. In the simple pole model we fit for the intercept and the pole mass  $m_{\text{pole}}$ , while in the modified pole model we fit for the intercept and the shape parameter  $\alpha$ , which summarizes the effective pole contribution. The results for all modes are summarized in Table VII. Comparisons of the four fits, for each of the four modes, are shown in Fig. 3. To allow systematic differences to be viewed clearly between the various parameterizations, we normalize the data and all fit results to the result of the three parameter series fit in each  $q^2$  interval.

For the series expansion, comparison of the two-parameter and three-parameter fits shows that our kaon data prefer a non-zero quadratic  $z$  term. The probability of  $\chi^2$  improves from 29% (22%) to 89% (44%) going from two to three terms in the series for the  $K^-$  ( $K^0$ ) fit. The pion measurements currently lack sensitiv-

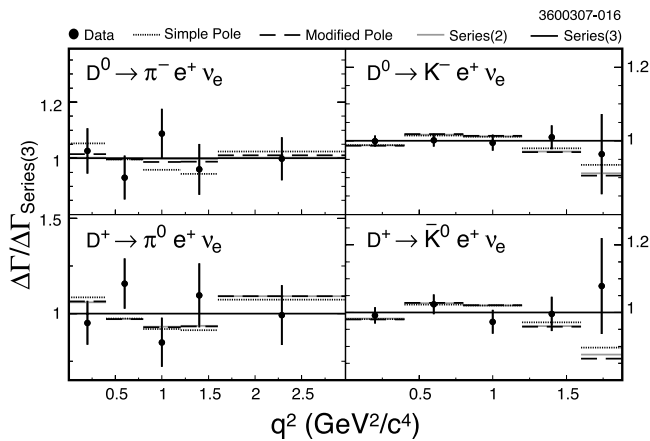


FIG. 3: Form factor fit comparison for all modes. All data (points) and fits (histograms) are normalized to the relevant three-parameter series fit result (Series(3), line at 1). The simple pole, modified pole, and two-parameter series fit (Series(2)) are shown by triple-dot-dash, dashed, and solid histograms, respectively.

ity to probe this term, and two and three parameter fits yield similar results for the first two parameters. Since a quadratic term appears to be preferred for the kaons, however, we include that term in our series fits to the pion data to improve the probability that our shape uncertainties bracket the true form factor shape. While the central value for  $a_2$  is an order of magnitude larger than the other terms, we stress that regions of parameter space with  $a_2$  of similar magnitude to  $a_0$  and  $a_1$  fall within the 90% hypercontour for the fit, so no strong statements can be made about the size of  $a_2$  or about the convergence (or potential lack thereof) of the series from these data.

For the pole models we observe that the parameterizations can provide a shape that describes our data adequately, but only with parameter values that do not support their physical basis. Although the fits give quite reasonable  $\chi^2$  values (see Table VII), the poles masses do not agree with the  $M_{D_s^*}$  ( $M_{D^*}$ ) masses expected for the kaon (pion) modes by over  $3\sigma$  for the most precise fits. The  $1 + 1/\beta - \delta$  results from the  $D^0 \rightarrow K^- e^+ \nu_e$  series expansion fit are over  $3\sigma$  from the value of  $\sim 2$  necessary for physical validity of the BK parameterization, while those derived from our  $\alpha$  values for the kaon modes are tens of  $\sigma$  away.

### VIII. EXTRACTION OF $|V_{cs}|$ AND $|V_{cd}|$

We extract  $|V_{cd}|$  and  $|V_{cs}|$  by combining our  $|V_{cq}|f_+(0)$  results from the three parameter series expansion fits with the unquenched LQCD results [2]  $f_+^{(D \rightarrow \pi)}(0) = 0.64(3)(6)$  and  $f_+^{(D \rightarrow K)}(0) = 0.73(3)(7)$ . For the  $D^0 \rightarrow \pi^-$  and  $D^+ \rightarrow \pi^0$  modes we find  $|V_{cd}| = 0.218 \pm 0.011 \pm$

$0.005 \pm 0.023$  and  $|V_{cd}| = 0.216 \pm 0.017 \pm 0.006 \pm 0.023$ , respectively. For the  $D^0 \rightarrow K^-$  and  $D^+ \rightarrow \bar{K}^0$  modes, we find  $|V_{cs}| = 1.023 \pm 0.013 \pm 0.013 \pm 0.107$  and  $|V_{cs}| = 1.004 \pm 0.020 \pm 0.015 \pm 0.105$ . Averaging the  $D^0$  and  $D^+$  results (taking into account correlated and uncorrelated uncertainties) we find

$$|V_{cd}| = 0.217 \pm 0.009 \pm 0.004 \pm 0.023 \quad (24)$$

and

$$|V_{cs}| = 1.015 \pm 0.010 \pm 0.011 \pm 0.106. \quad (25)$$

The uncertainties, statistical, systematic and theoretical, respectively, are dominated by the discretization uncertainty in the LQCD charm quark action, which should be improved in the near future for the Fermilab action, or greatly reduced through the use of other actions..

We can also extract the ratio  $|V_{cd}|/|V_{cs}|$  from the ratio of our measured form factors. From the  $z$  expansion fits to our  $D^0$  data, we obtain  $|V_{cd}|f_+^{(D \rightarrow \pi)}(0)/|V_{cs}|f_+^{(D \rightarrow K)}(0) = 0.187 \pm 0.010 \pm 0.003$ , while from our  $D^\pm$  data we obtain  $|V_{cd}|f_+^{(D \rightarrow \pi)}(0)/|V_{cs}|f_+^{(D \rightarrow K)}(0) = 0.188 \pm 0.015 \pm 0.004$ . The errors are statistical and systematic, respectively, and all correlations have been taken into account. Averaging, again with correlated uncertainties accounted for, we obtain

$$\frac{|V_{cd}|f_+^{(D \rightarrow \pi)}(0)}{|V_{cs}|f_+^{(D \rightarrow K)}(0)} = 0.188 \pm 0.008 \pm 0.002. \quad (26)$$

We can combine this result with calculations of  $f(0)^{(D \rightarrow \pi)}/f(0)^{(D \rightarrow K)}$  to obtain the ratio of CKM elements. A recent light cone sum rules (LCSR) calculation, for example, obtains [15]  $f_+^{(D \rightarrow \pi)}(0)/f_+^{(D \rightarrow K)}(0) = 0.84 \pm 0.04$ , which implies

$$\frac{|V_{cd}|}{|V_{cs}|} = 0.223 \pm 0.010_{\text{stat}} \pm 0.003_{\text{sys}} \pm 0.011_{\text{LCSR}}. \quad (27)$$

### IX. SUMMARY

In summary, we have measured branching fractions and branching-fraction ratios for four semileptonic  $D$  decay modes in five  $q^2$  bins. The branching fraction results are the most precise measured to date and agree well with world averages [4]. Our modified pole  $\alpha$  parameter results agree within  $1.3\sigma$  with previous determinations by CLEO III [16], FOCUS [17], and  $Ke\nu$  results from Belle [18], but show over  $3\sigma$  disagreement with Belle  $K\mu\nu$  results and LQCD fits. The  $\alpha$  parameters obtained with our individual  $Ke\nu$  results are separated from the recent BaBar result [19] by about  $2.5\sigma$ . The  $z$  expansion results between BaBar and our  $Ke\nu$  agree closer to the  $2\sigma$  level or better, depending on the level of correlation between the BaBar  $r_1$  and  $r_2$  parameters. The discrepancy

with LQCD is difficult to quantify because the covariance matrix for the LQCD form factors is lost during the chiral extrapolation procedure for the published analysis [2]. We have made the most precise CKM determinations from  $D$  semileptonic decays to date, and the results agree very well with neutrino based determinations of  $|V_{cd}|$  and charmed-tagged  $W$  decay measurements of  $|V_{cs}|$  [4]. Overall, these measurements represent a marked improvement in our knowledge of  $D$  semileptonic decay.

We gratefully acknowledge the effort of the CESR staff in providing us with excellent luminosity and running conditions. D. Cronin-Hennessy and A. Ryd thank the A.P. Sloan Foundation. This work was supported by the National Science Foundation, the U.S. Department of Energy, and the Natural Sciences and Engineering Research Council of Canada.

## APPENDIX A: THE $z$ -EXPANSION: DETAILED FORMS AND ALTERNATE RESULTS

The standard choice for the outer function  $\phi(t, t_0)$  in the  $z$  expansion for  $f_+(q^2)$  (Eq. 12) arises from considerations of unitarity. From a perturbative Operator Product Expansion (OPE) calculation, one can show [9, 10, 31] that the choice

$$\phi(t, t_0) = \alpha \left( \sqrt{t_+ - t} + \sqrt{t_+ - t_0} \right) \times \frac{t_+ - t}{(t_+ - t_0)^{1/4}} \frac{(\sqrt{t_+ - t} + \sqrt{t_+ - t_-})^{3/2}}{(\sqrt{t_+ - t} + \sqrt{t_+})^5} \quad (\text{A1})$$

leads to a constraint on the coefficients

$$\sum_{k=0}^{n_a} a_k^2 \leq 1, \quad (\text{A2})$$

for any choice of  $n_a$ . The bound corresponds to forbidding the production rate of  $D\pi$  states by the relevant current to exceed the inclusive production rate, which can be calculated within the OPE. To leading order, the coefficient  $\alpha$  is given by

$$\alpha = \sqrt{\frac{\pi m_c^2}{3}}. \quad (\text{A3})$$

Numerically, we have taken the charm quark mass to be  $m_c = 1.2$  GeV.

The choice of the parameter  $t_0$  within the  $z$ -expansion provides a potential source of ambiguity when comparing experimental results. In our fits, we have, for simplicity, chosen  $t_0 = 0$  in our form factor fits utilizing the  $z$ -expansion. Another common choice for  $t_0$  is that which minimizes the maximal value of the mapping  $z(q^2)$  over the entire physical range. The value  $t_0 = t_+ \left( 1 - \sqrt{1 - t_-/t_+} \right)$ , where  $t_{\pm} = m_D \pm m_{K,\pi}$  accomplishes this minimization. The best fit  $a_i$  values for our three parameter fit using this alternate value for  $t_0$  are presented in Table VIII. The values for  $|V_{cq}|f_+(0)$  ( $q = s, d$ ) that we find in these fits are identical, within the precision we are quoting, to those presented in Table VII.

Finally, some experimental results for the  $z$ -expansion are presented in terms of the ratios  $r_i = a_i/a_0$  for  $i > 0$ . To allow straightforward comparison, we also quote our results in this form in Table VIII.

## APPENDIX B: CORRELATION MATRICES

To allow complete external use of the partial branching fractions presented in this paper, we present the statistical and systematic uncertainty correlation matrices. These matrices will allow, for example, for simultaneous fits of these results with other experimental results to obtain form factor parameters. The statistical correlation matrix (Table IX) is derived from the  $20 \times 20$  covariance matrix produced in our fitting procedure.

To obtain the systematic correlation matrix (Table X), we create a separate covariance matrix from the correlated motions of all 20 yields in each individual systematic study. We then sum the resulting matrices to obtain the total systematic covariance matrix. In the absence of correlations, this procedure would reduce to adding the systematic contributions for a given measurement in quadrature. In producing the covariance matrix for the form factor systematic uncertainty, we assume that the two pion modes are fully correlated and similarly for the two kaon modes, but treat the pion and kaon uncertainties as uncorrelated. For the  $N_{D^+D^-}$  and  $N_{D^0\bar{D}^0}$  uncertainties, we take into account the 39% correlation in those yields.

- 
- [1] M. Kobayashi and T. Maskawa, *Prog. Theor. Phys.* **49**, 652 (1973).  
[2] C. Aubin *et al.*, *Phys. Rev. Lett.* **94**, 011601 (2005).  
[3] R. A. Briere *et al.* (CESR-c and CLEO-c Taskforces, CLEO-c Collaboration), Cornell University, LEPP Report No. CLNS 01/1742 (2001) (unpublished).  
[4] W. M. Yao *et al.*, *J. Phys. G* **33**, 1 (2006).  
[5] D. Cronin-Hennessy *et al.* [CLEO Collaboration], LEPP Report No. CLNS 06/1967 (2006).  
[6] G. S. Huang *et al.* [CLEO Collaboration], *Phys. Rev. Lett.* **95**, 181801 (2005); T. E. Coan *et al.*, *Phys. Rev. Lett.* **95**, 181802 (2005).  
[7] J. D. Richman and P. R. Burchat, *Rev. Mod. Phys.* **67**, 893 (1995).



TABLE VIII: The fit results for the 3 parameter  $z$ -expansion fit for both  $t_0 = 0$  and  $t_0 = t_+ \left(1 - \sqrt{1 - t_-/t_+}\right)$ . The fit results are also presented in terms of the ratios  $r_i = a_i/a_0$  for  $i = 1, 2$ .

|   |                       | $a_0$        | $a_1$          | $a_2$          | $\rho_{01}$ | $\rho_{02}$ | $\rho_{12}$ |
|---|-----------------------|--------------|----------------|----------------|-------------|-------------|-------------|
| $t_0 = 0$                                       | $\pi^- e^+ \nu_e$     | 0.044(2)(1)  | -0.18(7)(2)    | -0.03(35)(12)  | 0.81        | 0.71        | 0.96        |
|   | $\pi^0 e^+ \nu_e$     | 0.044(3)(1)  | -0.23(11)(2)   | -0.60(57)(15)  | 0.80        | 0.67        | 0.95        |
|   | $K^- e^+ \nu_e$       | 0.0234(3)(3) | -0.009(21)(7)  | 0.52(28)(6)    | 0.62        | 0.56        | 0.96        |
|   | $\bar{K}^0 e^+ \nu_e$ | 0.0224(4)(3) | 0.009(32)(7)   | 0.76(42)(8)    | 0.72        | 0.64        | 0.96        |
| $t_0 = 0$                                       |                       | $a_0$        | $r_1$          | $r_2$          | $\rho_{01}$ | $\rho_{02}$ | $\rho_{12}$ |
|   | $\pi^- e^+ \nu_e$     | 0.044(2)(1)  | -4.1(1.7)(0.6) | -0.7(8.0)(2.9) | 0.85        | 0.71        | 0.95        |
|   | $\pi^0 e^+ \nu_e$     | 0.044(3)(1)  | -5.3(2.8)(0.5) | -14(14)(3)     | 0.85        | 0.71        | 0.95        |
|   | $K^- e^+ \nu_e$       | 0.0234(3)(3) | -0.4(9)(3)     | 22(12)(2)      | 0.62        | 0.54        | 0.95        |
| $t_0 = t_+ \left(1 - \sqrt{1 - t_-/t_+}\right)$ |                       | $a_0$        | $a_1$          | $a_2$          | $\rho_{01}$ | $\rho_{02}$ | $\rho_{12}$ |
|   | $\pi^- e^+ \nu_e$     | 0.072(2)(1)  | -0.15(5)(2)    | -0.09(35)(13)  | -0.48       | 0.21        | -0.94       |
|   | $\pi^0 e^+ \nu_e$     | 0.065(4)(1)  | -0.01(10)(2)   | -0.63(57)(14)  | -0.65       | 0.41        | -0.95       |
|   | $K^- e^+ \nu_e$       | 0.0252(2)(3) | -0.062(10)(2)  | 0.52(28)(6)    | -0.14       | -0.24       | -0.79       |
| $t_0 = t_+ \left(1 - \sqrt{1 - t_-/t_+}\right)$ |                       | $a_0$        | $r_1$          | $r_2$          | $\rho_{01}$ | $\rho_{02}$ | $\rho_{12}$ |
|   | $\pi^- e^+ \nu_e$     | 0.072(2)(1)  | -2.1(7)(3)     | -1.2(4.8)(1.7) | -0.41       | 0.22        | -0.96       |
|   | $\pi^0 e^+ \nu_e$     | 0.065(4)(1)  | -0.2(1.5)(4)   | -9.8(9.1)(2.1) | -0.64       | 0.47        | -0.97       |
|   | $K^- e^+ \nu_e$       | 0.0252(2)(3) | -2.4(4)(1)     | 21(11)(2)      | -0.05       | -0.27       | -0.81       |
| $t_0 = t_+ \left(1 - \sqrt{1 - t_-/t_+}\right)$ |                       | $a_0$        | $r_1$          | $r_2$          | $\rho_{01}$ | $\rho_{02}$ | $\rho_{12}$ |
|   | $\pi^- e^+ \nu_e$     | 0.072(2)(1)  | -2.1(7)(3)     | -1.2(4.8)(1.7) | -0.41       | 0.22        | -0.96       |
|   | $\pi^0 e^+ \nu_e$     | 0.065(4)(1)  | -0.2(1.5)(4)   | -9.8(9.1)(2.1) | -0.64       | 0.47        | -0.97       |
|   | $K^- e^+ \nu_e$       | 0.0252(2)(3) | -2.4(4)(1)     | 21(11)(2)      | -0.05       | -0.27       | -0.81       |
| $t_0 = t_+ \left(1 - \sqrt{1 - t_-/t_+}\right)$ |                       | $a_0$        | $r_1$          | $r_2$          | $\rho_{01}$ | $\rho_{02}$ | $\rho_{12}$ |
|   | $\pi^- e^+ \nu_e$     | 0.072(2)(1)  | -2.1(7)(3)     | -1.2(4.8)(1.7) | -0.41       | 0.22        | -0.96       |
|   | $\pi^0 e^+ \nu_e$     | 0.065(4)(1)  | -0.2(1.5)(4)   | -9.8(9.1)(2.1) | -0.64       | 0.47        | -0.97       |
|   | $K^- e^+ \nu_e$       | 0.0252(2)(3) | -2.4(4)(1)     | 21(11)(2)      | -0.05       | -0.27       | -0.81       |
| $t_0 = t_+ \left(1 - \sqrt{1 - t_-/t_+}\right)$ |                       | $a_0$        | $r_1$          | $r_2$          | $\rho_{01}$ | $\rho_{02}$ | $\rho_{12}$ |
|   | $\pi^- e^+ \nu_e$     | 0.072(2)(1)  | -2.1(7)(3)     | -1.2(4.8)(1.7) | -0.41       | 0.22        | -0.96       |
|   | $\pi^0 e^+ \nu_e$     | 0.065(4)(1)  | -0.2(1.5)(4)   | -9.8(9.1)(2.1) | -0.64       | 0.47        | -0.97       |
|   | $K^- e^+ \nu_e$       | 0.0252(2)(3) | -2.4(4)(1)     | 21(11)(2)      | -0.05       | -0.27       | -0.81       |
| $t_0 = t_+ \left(1 - \sqrt{1 - t_-/t_+}\right)$ |                       | $a_0$        | $r_1$          | $r_2$          | $\rho_{01}$ | $\rho_{02}$ | $\rho_{12}$ |
|   | $\pi^- e^+ \nu_e$     | 0.072(2)(1)  | -2.1(7)(3)     | -1.2(4.8)(1.7) | -0.41       | 0.22        | -0.96       |
|   | $\pi^0 e^+ \nu_e$     | 0.065(4)(1)  | -0.2(1.5)(4)   | -9.8(9.1)(2.1) | -0.64       | 0.47        | -0.97       |
|   | $K^- e^+ \nu_e$       | 0.0252(2)(3) | -2.4(4)(1)     | 21(11)(2)      | -0.05       | -0.27       | -0.81       |
| $t_0 = t_+ \left(1 - \sqrt{1 - t_-/t_+}\right)$ |                       | $a_0$        | $r_1$          | $r_2$          | $\rho_{01}$ | $\rho_{02}$ | $\rho_{12}$ |
|   | $\pi^- e^+ \nu_e$     | 0.072(2)(1)  | -2.1(7)(3)     | -1.2(4.8)(1.7) | -0.41       | 0.22        | -0.96       |
|   | $\pi^0 e^+ \nu_e$     | 0.065(4)(1)  | -0.2(1.5)(4)   | -9.8(9.1)(2.1) | -0.64       | 0.47        | -0.97       |
|   | $K^- e^+ \nu_e$       | 0.0252(2)(3) | -2.4(4)(1)     | 21(11)(2)      | -0.05       | -0.27       | -0.81       |
| $t_0 = t_+ \left(1 - \sqrt{1 - t_-/t_+}\right)$ |                       | $a_0$        | $r_1$          | $r_2$          | $\rho_{01}$ | $\rho_{02}$ | $\rho_{12}$ |
|   | $\pi^- e^+ \nu_e$     | 0.072(2)(1)  | -2.1(7)(3)     | -1.2(4.8)(1.7) | -0.41       | 0.22        | -0.96       |
|   | $\pi^0 e^+ \nu_e$     | 0.065(4)(1)  | -0.2(1.5)(4)   | -9.8(9.1)(2.1) | -0.64       | 0.47        | -0.97       |
|   | $K^- e^+ \nu_e$       | 0.0252(2)(3) | -2.4(4)(1)     | 21(11)(2)      | -0.05       | -0.27       | -0.81       |
| $t_0 = t_+ \left(1 - \sqrt{1 - t_-/t_+}\right)$ |                       | $a_0$        | $r_1$          | $r_2$          | $\rho_{01}$ | $\rho_{02}$ | $\rho_{12}$ |
|   | $\pi^- e^+ \nu_e$     | 0.072(2)(1)  | -2.1(7)(3)     | -1.2(4.8)(1.7) | -0.41       | 0.22        | -0.96       |
|   | $\pi^0 e^+ \nu_e$     | 0.065(4)(1)  | -0.2(1.5)(4)   | -9.8(9.1)(2.1) | -0.64       | 0.47        | -0.97       |
|   | $K^- e^+ \nu_e$       | 0.0252(2)(3) | -2.4(4)(1)     | 21(11)(2)      | -0.05       | -0.27       | -0.81       |
| $t_0 = t_+ \left(1 - \sqrt{1 - t_-/t_+}\right)$ |                       | $a_0$        | $r_1$          | $r_2$          | $\rho_{01}$ | $\rho_{02}$ | $\rho_{12}$ |
|   | $\pi^- e^+ \nu_e$     | 0.072(2)(1)  | -2.1(7)(3)     | -1.2(4.8)(1.7) | -0.41       | 0.22        | -0.96       |
|   | $\pi^0 e^+ \nu_e$     | 0.065(4)(1)  | -0.2(1.5)(4)   | -9.8(9.1)(2.1) | -0.64       | 0.47        | -0.97       |
|   | $K^- e^+ \nu_e$       | 0.0252(2)(3) | -2.4(4)(1)     | 21(11)(2)      | -0.05       | -0.27       | -0.81       |
| $t_0 = t_+ \left(1 - \sqrt{1 - t_-/t_+}\right)$ |                       | $a_0$        | $r_1$          | $r_2$          | $\rho_{01}$ | $\rho_{02}$ | $\rho_{12}$ |
|   | $\pi^- e^+ \nu_e$     | 0.072(2)(1)  | -2.1(7)(3)     | -1.2(4.8)(1.7) | -0.41       | 0.22        | -0.96       |
|   | $\pi^0 e^+ \nu_e$     | 0.065(4)(1)  | -0.2(1.5)(4)   | -9.8(9.1)(2.1) | -0.64       | 0.47        | -0.97       |
|   | $K^- e^+ \nu_e$       | 0.0252(2)(3) | -2.4(4)(1)     | 21(11)(2)      | -0.05       | -0.27       | -0.81       |
| $t_0 = t_+ \left(1 - \sqrt{1 - t_-/t_+}\right)$ |                       | $a_0$        | $r_1$          | $r_2$          | $\rho_{01}$ | $\rho_{02}$ | $\rho_{12}$ |
|   | $\pi^- e^+ \nu_e$     | 0.072(2)(1)  | -2.1(7)(3)     | -1.2(4.8)(1.7) | -0.41       | 0.22        | -0.96       |
|   | $\pi^0 e^+ \nu_e$     | 0.065(4)(1)  | -0.2(1.5)(4)   | -9.8(9.1)(2.1) | -0.64       | 0.47        | -0.97       |
|   | $K^- e^+ \nu_e$       | 0.0252(2)(3) | -2.4(4)(1)     | 21(11)(2)      | -0.05       | -0.27       | -0.81       |
| $t_0 = t_+ \left(1 - \sqrt{1 - t_-/t_+}\right)$ |                       | $a_0$        | $r_1$          | $r_2$          | $\rho_{01}$ | $\rho_{02}$ | $\rho_{12}$ |
|   | $\pi^- e^+ \nu_e$     | 0.072(2)(1)  | -2.1(7)(3)     | -1.2(4.8)(1.7) | -0.41       | 0.22        | -0.96       |
|   | $\pi^0 e^+ \nu_e$     | 0.065(4)(1)  | -0.2(1.5)(4)   | -9.8(9.1)(2.1) | -0.64       | 0.47        | -0.97       |
|   | $K^- e^+ \nu_e$       | 0.0252(2)(3) | -2.4(4)(1)     | 21(11)(2)      | -0.05       | -0.27       | -0.81       |

- [8] D. Becirevic and A. B. Kaidalov, Phys. Lett. **B478**, 417 (2000).  
[9] C. G. Boyd, B. Grinstein and R. F. Lebed, Phys. Rev. Lett. **74**, 4603 (1995).  
[10] C. G. Boyd and M. J. Savage, Phys. Rev. D **56**, 303 (1997).  
[11] C. M. Arnesen, B. Grinstein, I. Z. Rothstein and I. W. Stewart, Phys. Rev. Lett. **95**, 071802 (2005).  
[12] T. Becher and R. J. Hill, Phys. Lett. B **633**, 61 (2006).  
[13] E. Gulez, A. Gray, M. Wingate, C. T. H. Davies, G. P. Lepage and J. Shigemitsu, Phys. Rev. D **73**, 074502 (2006).  
[14] R. J. Hill, FPCP, Vancouver (2006), hep-ph/0606023.  
[15] P. Ball, Phys. Lett. B **641**, 50 (2006).  
[16] G. S. Huang *et al.* [CLEO Collaboration], Phys. Rev. Lett. **94**, 011802 (2005).  
[17] J. M. Link *et al.* [FOCUS Collaboration], Phys. Lett. B **607**, 233 (2005).  
[18] L. Widhalm *et al.* [Belle Collaboration], Phys. Rev. Lett. **97**, 061804 (2006).  
[19] B. Aubert *et al.* [BABAR Collaboration], Phys. Rev. D **76**, 052005 (2007).  
[20] S. B. Athar *et al.* [CLEO Collaboration], Phys. Rev. D **68**, 072003 (2003).  
[21] G. Viehhauser, Nucl. Instrum. Methods A **462**, 146 (2001); D. Peterson *et al.*, Nucl. Instrum. Methods Phys. Res., Sect. A **478**, 142 (2002).  
[22] CLEO Collaboration, M. Artuso *et al.*, Nucl. Instrum. Meth. Phys. Res., Sect. A **554**, 147 (2005).  
[23] R. Brun *et al.*, CERN DD/EE/84-1 (1987).  
[24] D.J. Lange, Nucl. Instrum. Methods Phys. Res., Sect. A **462**, 152 (2001).  
[25] Spurious CsI showers from hadronic interactions add linearly to  $E_{\text{miss}}$  but tend to average out in the vector sum for  $\vec{p}_{\text{miss}}$ . Incorrect mass assignment also smears  $E_{\text{miss}}$ .  
[26] R. Barlow and C. Beeston, Comput. Phys. Commun. **77**, 219 (1993).  
[27] PHOTOS v2.0, E. Barberio and Z. Was, Comput. Phys. Commun. **79**, 291 (1994).  
[28] T. C. Andre, Annals Phys. **322** (2007) 2518; T. Alexopoulos *et al.*, Phys. Rev. D **71**, 012001 (2005).  
[29] D. Scora and N. Isgur, Phys. Rev. D **52**, 2783 (1995).  
[30] S. Dobbs *et al.* [CLEO Collaboration], arXiv:0709.3783.  
[31] C. Bourrely, B. Machet and E. de Rafael, Nucl. Phys. B **189**, 157 (1981).

TABLE IX: The statistical correlation matrix obtained from the simultaneous fit to the data (see Section IV B). The lines indicate the mode boundaries. The modes are labeled by their final state hadron. Within each submode, the five  $q^2$  intervals are ordered from lowest to highest.

|             |       |        |         |        |        |        |         |        |        |        |        |        |        |        |        |             |        |        |        |        |
|-------------|-------|--------|---------|--------|--------|--------|---------|--------|--------|--------|--------|--------|--------|--------|--------|-------------|--------|--------|--------|--------|
|             |       |        | $\pi^-$ |        |        |        | $\pi^0$ |        |        |        |        | $K^-$  |        |        |        | $\bar{K}^0$ |        |        |        |        |
|             | 1.000 | -0.047 | 0.034   | 0.025  | 0.030  | -0.002 | 0.002   | 0.003  | 0.004  | 0.002  | -0.059 | 0.003  | 0.002  | 0.002  | 0.000  | -0.010      | 0.006  | 0.009  | 0.010  | 0.006  |
| $\pi^-$     |       | 1.000  | -0.045  | 0.034  | 0.035  | 0.001  | -0.005  | 0.003  | 0.006  | 0.004  | -0.007 | -0.026 | 0.004  | 0.003  | 0.000  | 0.002       | -0.014 | 0.011  | 0.014  | 0.009  |
|             |       |        | 1.000   | -0.044 | 0.034  | 0.001  | 0.002   | -0.008 | 0.004  | 0.006  | 0.000  | -0.009 | -0.013 | 0.001  | 0.000  | 0.004       | 0.003  | -0.019 | 0.011  | 0.010  |
|             |       |        |         | 1.000  | -0.016 | 0.001  | 0.002   | 0.004  | -0.022 | 0.006  | -0.001 | 0.000  | -0.009 | -0.011 | 0.001  | 0.002       | 0.007  | -0.003 | -0.038 | -0.001 |
|             |       |        |         |        | 1.000  | -0.001 | -0.001  | -0.001 | 0.007  | -0.115 | -0.002 | -0.002 | -0.003 | -0.021 | -0.030 | -0.004      | -0.002 | -0.004 | -0.022 | -0.053 |
| $\pi^0$     |       |        |         |        | 1.000  | -0.089 | 0.033   | 0.017  | 0.018  | 0.000  | 0.000  | 0.000  | 0.000  | -0.001 | -0.013 | 0.006       | 0.005  | 0.004  | 0.001  |        |
|             |       |        |         |        |        | 1.000  | -0.094  | 0.032  | 0.023  | 0.001  | -0.001 | 0.000  | 0.001  | 0.000  | -0.006 | -0.010      | 0.006  | 0.004  | 0.001  |        |
|             |       |        |         |        |        |        | 1.000   | -0.090 | 0.032  | 0.001  | 0.001  | -0.002 | 0.001  | 0.000  | 0.004  | -0.006      | -0.016 | 0.002  | 0.002  |        |
|             |       |        |         |        |        |        |         | 1.000  | -0.069 | 0.001  | 0.001  | 0.000  | -0.004 | -0.002 | 0.002  | 0.004       | -0.013 | -0.029 | -0.005 |        |
| $K^-$       |       |        |         |        |        |        |         |        |        |        | 1.000  | -0.064 | 0.023  | 0.017  | 0.012  | -0.033      | 0.006  | 0.005  | 0.005  | 0.002  |
|             |       |        |         |        |        |        |         |        |        |        |        | 1.000  | -0.070 | 0.021  | 0.011  | 0.002       | -0.019 | 0.006  | 0.007  | 0.003  |
|             |       |        |         |        |        |        |         |        |        |        |        |        | 1.000  | -0.071 | 0.013  | 0.007       | 0.005  | -0.021 | 0.001  | 0.002  |
|             |       |        |         |        |        |        |         |        |        |        |        |        |        | 1.000  | -0.094 | 0.005       | 0.007  | 0.000  | -0.040 | -0.016 |
| $\bar{K}^0$ |       |        |         |        |        |        |         |        |        |        |        |        |        |        |        | 1.000       | -0.068 | 0.031  | 0.019  | 0.007  |
|             |       |        |         |        |        |        |         |        |        |        |        |        |        |        |        |             | 1.000  | -0.060 | 0.027  | 0.009  |
|             |       |        |         |        |        |        |         |        |        |        |        |        |        |        |        |             |        | 1.000  | -0.068 | 0.011  |
|             |       |        |         |        |        |        |         |        |        |        |        |        |        |        |        |             |        |        | 1.000  | -0.098 |
|             |       |        |         |        |        |        |         |        |        |        |        |        |        |        |        |             |        |        |        | 1.000  |

TABLE X: The total systematic correlation matrix for the 20 measured mode /  $q^2$  intervals (see Section V). The lines indicate the mode boundaries. The modes are labeled by their final state hadron. Within each mode, the five  $q^2$  intervals are ordered from lowest to highest.

|             |      |      |         |      |      |      |         |      |      |       |      |       |      |      |      |             |      |      |      |       |      |
|-------------|------|------|---------|------|------|------|---------|------|------|-------|------|-------|------|------|------|-------------|------|------|------|-------|------|
|             |      |      | $\pi^-$ |      |      |      | $\pi^0$ |      |      |       |      | $K^-$ |      |      |      | $\bar{K}^0$ |      |      |      |       |      |
|             | 1.00 | 0.73 | 0.64    | 0.59 | 0.51 | 0.45 | 0.29    | 0.13 | 0.28 | 0.06  | 0.75 | 0.59  | 0.56 | 0.53 | 0.59 | 0.34        | 0.27 | 0.22 | 0.26 | 0.26  |      |
| $\pi^-$     |      | 1.00 | 0.87    | 0.81 | 0.56 | 0.13 | 0.33    | 0.21 | 0.34 | -0.04 | 0.75 | 0.74  | 0.74 | 0.70 | 0.63 | 0.28        | 0.32 | 0.32 | 0.26 | 0.13  |      |
|             |      |      | 1.00    | 0.94 | 0.46 | 0.23 | 0.55    | 0.34 | 0.39 | -0.20 | 0.79 | 0.86  | 0.86 | 0.85 | 0.64 | 0.25        | 0.32 | 0.28 | 0.19 | -0.10 |      |
|             |      |      |         | 1.00 | 0.46 | 0.19 | 0.61    | 0.38 | 0.44 | -0.21 | 0.77 | 0.89  | 0.89 | 0.91 | 0.65 | 0.23        | 0.30 | 0.27 | 0.17 | -0.11 |      |
|             |      |      |         |      | 1.00 | 0.05 | 0.14    | 0.08 | 0.10 | 0.24  | 0.57 | 0.52  | 0.52 | 0.50 | 0.56 | 0.20        | 0.18 | 0.19 | 0.22 | 0.37  |      |
| $\pi^0$     |      |      |         |      | 1.00 | 0.70 | 0.77    | 0.68 | 0.41 | 0.35  | 0.27 | 0.24  | 0.22 | 0.20 | 0.56 | 0.53        | 0.47 | 0.49 | 0.31 |       |      |
|             |      |      |         |      |      | 1.00 | 0.83    | 0.75 | 0.01 | 0.46  | 0.58 | 0.57  | 0.62 | 0.32 | 0.56 | 0.62        | 0.56 | 0.46 | 0.07 |       |      |
|             |      |      |         |      |      |      | 1.00    | 0.71 | 0.31 | 0.28  | 0.37 | 0.36  | 0.39 | 0.19 | 0.40 | 0.45        | 0.42 | 0.34 | 0.07 |       |      |
|             |      |      |         |      |      |      |         | 1.00 | 0.36 | 0.44  | 0.49 | 0.48  | 0.48 | 0.31 | 0.64 | 0.70        | 0.68 | 0.63 | 0.32 |       |      |
| $K^-$       |      |      |         |      |      |      |         |      |      |       |      |       |      |      |      |             |      |      |      |       |      |
|             |      |      |         |      |      |      |         |      |      |       | 1.00 | 0.93  | 0.92 | 0.86 | 0.75 | 0.40        | 0.39 | 0.35 | 0.30 | 0.11  |      |
|             |      |      |         |      |      |      |         |      |      |       |      | 1.00  | 0.98 | 0.81 | 0.33 | 0.40        | 0.38 | 0.31 | 0.03 |       |      |
|             |      |      |         |      |      |      |         |      |      |       |      |       | 1.00 | 0.98 | 0.82 | 0.33        | 0.40 | 0.38 | 0.31 | 0.05  |      |
| $\bar{K}^0$ |      |      |         |      |      |      |         |      |      |       |      |       |      |      |      |             |      |      |      |       |      |
|             |      |      |         |      |      |      |         |      |      |       |      |       |      |      |      | 1.00        | 0.96 | 0.94 | 0.88 | 0.62  |      |
|             |      |      |         |      |      |      |         |      |      |       |      |       |      |      |      |             | 1.00 | 0.99 | 0.94 | 0.63  |      |
|             |      |      |         |      |      |      |         |      |      |       |      |       |      |      |      |             |      | 1.00 | 0.96 | 0.67  |      |
|             |      |      |         |      |      |      |         |      |      |       |      |       |      |      |      |             |      |      | 1.00 | 0.80  |      |
|             |      |      |         |      |      |      |         |      |      |       |      |       |      |      |      |             |      |      |      |       | 1.00 |